universität wien

DIPLOMARBEIT

Titel der Diplomarbeit

3D SEISMIC VELOCITY AND ATTENUATION MODEL OF THE VIENNA BASIN

Verfasser

Stefan Pfeiler

angestrebter akademischer Grad

Magister der Naturwissenschaften (Mag. rer. nat)

Wien, 2012

Studienkennzahl lt. Studienblatt:	A 416
Studienrichtung lt. Studienblatt:	Diplomstudium Geophysik
Betreuerin / Betreuer:	O. Univ. Prof. DI. Dr. Ewald Brückl

3D GESCHWINDIGKEITS- UND DÄMPFUNGS MODELL DES WIENER BECKENS

Eine Untersuchung im Auftrag der OMV

ZUSAMMENFASSUNG

Das im nordöstlichen Teil Österreichs liegende Wiener Becken besteht aus drei Stockwerken. Zuoberst liegt die sedimentäre Beckenfüllung des *Neogens*, die darunter liegenden *Nördlichen Kalkalpen* als Teil des alpin-karpathischen Überschiebungsgürtels und als unterstes Stockwerk das *subalpin-karpathische Mesozoikum*. Die weitreichenden Explorationstätigkeiten sowie ergiebige Öl- und Gasförderungen der letzten Jahrzehnte durch die OMV ergaben eine hinreichend genaue Vorstellung über den Aufbau des Neogens. In jüngster Vergangenheit jedoch rückten die Nördlichen Kalkalpen in den Mittelpunkt des Interesses. In den komplex gefalteten Strukturen dieses Gebietes besteht eine erhöhte Höffigkeit reichhaltige Kohlenwasserstoffreservoirs vorzufinden. Der für eine genaue räumliche Auflösung unerlässliche Anteil an hohen Frequenzen fehlt aber in den seismische Signalen aus großen Tiefen. Daher zeichnete die Analyse von seismischen Daten bisher nur ein unzureichendes Bild der geologischen Formationen unterhalb des Beckenbodens des Neogens. Für ein detailgenaueres Bild ist eine zielorientierte seismische Akquisition notwendig, für das Design einer solchen bedarf es eines verbesserten Geschwindigkeitsmodells.
Das Ziel dieser Arbeit ist es ein Modell des Wiener Beckens zu erstellen, das sowohl geologische Strukturen, Geschwindigkeitsinformationen als auch Absorptionsparameter enthält. Der strukturelle Aufbau des Modells entspricht im Wesentlichen den bekannten Vorstellungen und wird um einige seismische Horizonte erweitert. Die Erstellung des Geschwindigkeitsmodells beruht auf der Auswertung von Checkshots und Sonic logs. Durch Analyse von VSP-Daten wird der seismische Qualitätsfaktor Q bestimmt und somit das Absorptionsverhalten des Untergrundes in das Modell eingebunden. Die Methoden der *spektralen Verhältnisse* und *spectral modelling* werden dabei angewandt und verglichen.

3D SEISMIC VELOCITY AND ATTENUATION MODEL OF THE VIENNA BASIN

An investigation conducted on behalf of OMV

OMV

ABSTRACT

The Vienna basin, located in the north east of Austria, consists of three major units. The *Neogene* Basin fill representing the actual Vienna Basin, the underlying *Northern Calcareous Alps* belonging to the alpine-carpathian thrust sheets and the undermost *subalpine-carpathian mesozoic* structures. Extensive exploration and hydrocarbon production activities by OMV have been conducted during the last decades in the sedimentary strata of the Neogene and yielded detailed information of geological structures and seismic velocity distribution in the Neogene section. In the recent past the focus of interest came to the deeply buried structures of the Northern Calcareous Alps, which are assumed to be an area of high hydrocarbon prospectivity. However, structures underneath the Neogene Basin fill are rather poorly resolved due to bad signal to noise ratio and the lack of high frequencies of seismic signals coming from greater depths. In order to image the geological structures underneath the basin floor of the Neogene it is necessary to design a target oriented seismic acquisition configuration. To set up such a configuration an improved seismic velocity model is required.

It is the objective of this diploma thesis to design a comprehensive model of the area of interest, which contains seismic velocities, known and estimated geological structures and attenuation information as well. The structural content of the model is based on a preliminary understanding of the deeply buried structures of the Vienna Basin and known seismic horizons as well. Information on seismic velocity is derived from sonic log and checkshots of two deep reaching boreholes. In order to quantify the intrinsic attenuation the seismic quality factor Q is determined. The analysis on is based vertical seismic profiling data and applies the spectral modelling and the spectral ratio method.

TABLE OF CONTENT

1 INTRODUCTION

1.1 MOTIVATION

The occurrence of oil and gas in the Vienna Basin is known since long times, commercial hydrocarbon production started at the beginning of the 20th century. During the last decades OMV carried out extensive exploration and production activities all over the Vienna Basin and discovered remarkable oil and gas reservoirs in the sedimentary deposits of the Neogene. In the recent past the focus of interest was set on the Northern Calcareous Alps underneath the Neogene Basin floor, especially the steep and complex structures of the Frankenfelser-Lunzer nappe are assumed to have considerable oil and gas reservoirs.

In the area of interest the Northern Calcareuos Alps appear at a depth of approximately 3000 meters underneath the tertiary sediments of the Neogene. Dozens of boreholes and previous three dimensional (3D) seismic data led to a detailed image of the Neogene. Due to the great depth only a limited number of wells are reaching the Northern Calcareous Alps in order to provide geological and geophysical data of deeper areas. Seismic signals from greater depths are suffering from low signal-to-noise ratio and the lack of short wavelengths as a consequence of frequency dependent attenuation, which makes seismic horizons and geological structures hard to interpret on seismic sections. In the Neogene the seismic velocity distribution is clearly defined by two given 3D velocity fields. Various seismic horizons mapped on 3D PSDM[1] sections represent the subsurface structures within the investigated area very well. The knowledge of the build-up of the Northern Calcareous Alps is mainly based on a preliminary understanding of the subsurface structure. Several deep reaching boreholes provide velocity information and vertical seismic profiling data as well.

So, while geophysical exploration yielded a detailed understanding of the sedimentary strata of the Neogene, the Northern Calcareous Alps are rather poorly explored. In order to address this problem and to illuminate the deeply buried structures underneath the basin floor OMV initiated a study to design a target oriented 3D seismic acquisition configuration.
This implies the need of an improved velocity model of the Vienna Basin in order to significantly enhance the quality of the configuration design. The OMV study is separated into two parts.

The first part, carried out by the author and presented in this thesis, comprises the definition and construction of a comprehensive model that contains information on seismic velocity distribution, structural information and parameters that quantify the seismic attenuation as well. The second part, carried out by Martin Fuchsluger, deals with the actual configuration of the seismic acquisition survey based on the comprehensive model of the Vienna Basin developed in this thesis.

1.2 OUTLINE OF THIS THESIS

After this introducing chapter an overview of the geological constitution, the tectonical development and the geographical setting of the Vienna Basin and the investigated area is given in chapter 2.

Chapter 3 encompasses theoretical consideration of seismic wave propagation and highlights some important velocity terms.

Sonic logs, checkshots and vertical seismic profiling are important issues within this thesis, thus chapter 4 is dedicated to different borehole measurements.

Chapter 5 deals with the principles of seismic migration, PSDM[1] and CRS[2] technology is briefly discussed in comparison.

Seismic waves are facing a continuous loss of amplitude as they are propagating through elastic media. In chapter 6 the theoretical background of amplitude decay is presented.

---

[1] Pre Stack Depth Migration
[2] Common Reflection Surface

In chapter 7 the available data and applied software tools are listed in detail.

Chapters 8 encompass the construction of the structural model. The constitution of the internal structure of the model is defined using given and estimated horizons of the Neogene and the Northern Calcareous Alps as well.

The analysis of velocity data coming from sonic logs and check shots is carried out in chapter 9. Also the construction and build-up of the final velocity model is presented and discussed.

In order to quantify the amplitude decay of a seismic wave as it travels from source to receiver, chapter 10 examines the intrinsic attenuation of the investigated area and determines the seismic quality factor Q. For analysis vertical seismic profiling data sets of two deep reaching boreholes are utilized. For Q value determination the spectral ratio method and the spectral modelling method is applied, the results are compared and discussed.

Finally, chapter 11 gives a conclusive summary of this thesis.

2 GEOLOGY OF THE VIENNA BASIN AND THE MATZEN AREA

The following chapter gives an overview of the Vienna Basin and the investigated area, its geological and stratigraphical constitution and tectonic development. Some facts of hydrocarbons are highligthed.

2.1 GEOGRAPHICAL SETTING

The Vienna Basin is located in between the Eastern Alps, the Western Carpathians and the western part of the Pannonian Basin. It ranges from Gloggnitz (Lower Austria) in the south to Napajedl (Czech republic) in the north and covers an area of approximately 200 km times 50 km. It can be separated into a larger Austrian part and a smaller Czech-Slovakian part, the river Danube divides the basin into the southern and the northern Vienna Basin (Wessely, 2006). The western border of the Vienna Basin is built by the units of the eastern margin of the Northern Alps: Grauwackenzone, Northern Calcareous Alps and Flyschzone. The northern boundary is formed by the Waschbergzone and Little Carpathian mountains. In the east the Vienna Basin is bordered by Hainburger mountains, the Leithagebirge and the Rosaliengebirge, which belong to the Central Alpine Carpathian zone (Piller 1999, Wessely 1988).

2.2 TECTONICAL DEVELOPMENT AND MAIN STRUCTURES

The shape and structure of the Vienna Basin can be interpreted as a result of tectonic motion lasting since 22.5 Ma. driven by the collision of the African plate and the European plate. It is part of the Parathethys, which was formed together with the Mediterranean Sea after the Thetys ocean has vanished in the late Eocene. The rhombic shape and the left stepping pattern of the main faults of the basin point to a pull-apart mechanism, which started at the end of the Early Miocene in the Karpathian.

Following Wessely (1993) the Vienna Basin can be subdivided vertically into three main floors

- 1st floor: the sedimentary strata of the Neogene basin fill, the actual Vienna Basin
- 2nd floor: the allochthonous alpine-carpathian thrust sheets
- 3rd floor: the autochthonous subalpin-carpathian Mesozoic

The sedimentary strata of the first floor reaches a maximum thickness of approximately 6000 meters. The oldest layers in the northern part were deposited during Eggenburgian and Ottnangian, sediments from Karpatian up to the Pontian period are established all over the Vienna Basin (see figure 2.1). Due to complex fault system the Neogene Basin fill is internally highly structured, where certain faults can cover remarkable vertical extensions. E.g. the *Leopoldsdorfer fault* in the south and the *Steinberg fault* in the north are reaching a vertical displacement of approximately 4000 respectively 6000 meters.

The *allochthonous alpin carpathian thrust belt*, the second floor, crosses the Vienna Basin below the Neogene Basin fill. It consits of several tectonic units, e.g. from north-west to south-east the *Flysch zone*, the *Northern Calcareous Alps*, the *Grauwacken* zone and the *Central Alpine* zone. The sediments have been mainly deposited during the paleogene and thrusted, driven by tectonic forces, over the autochthonous Mesozoic and are therefore called *allochthonous*.

The third floor and undermost part of the Vienna Basin is the *autochthonous subalpin carpathian Mesozoic*, which consists of the Bohemian massif, the Mesozoic cover and the Molasse Basin sediments (Hamilton et al 1999; Rögl 1999; Kreutzer 1993; Piller 1999; Wessely 1993, 2006).

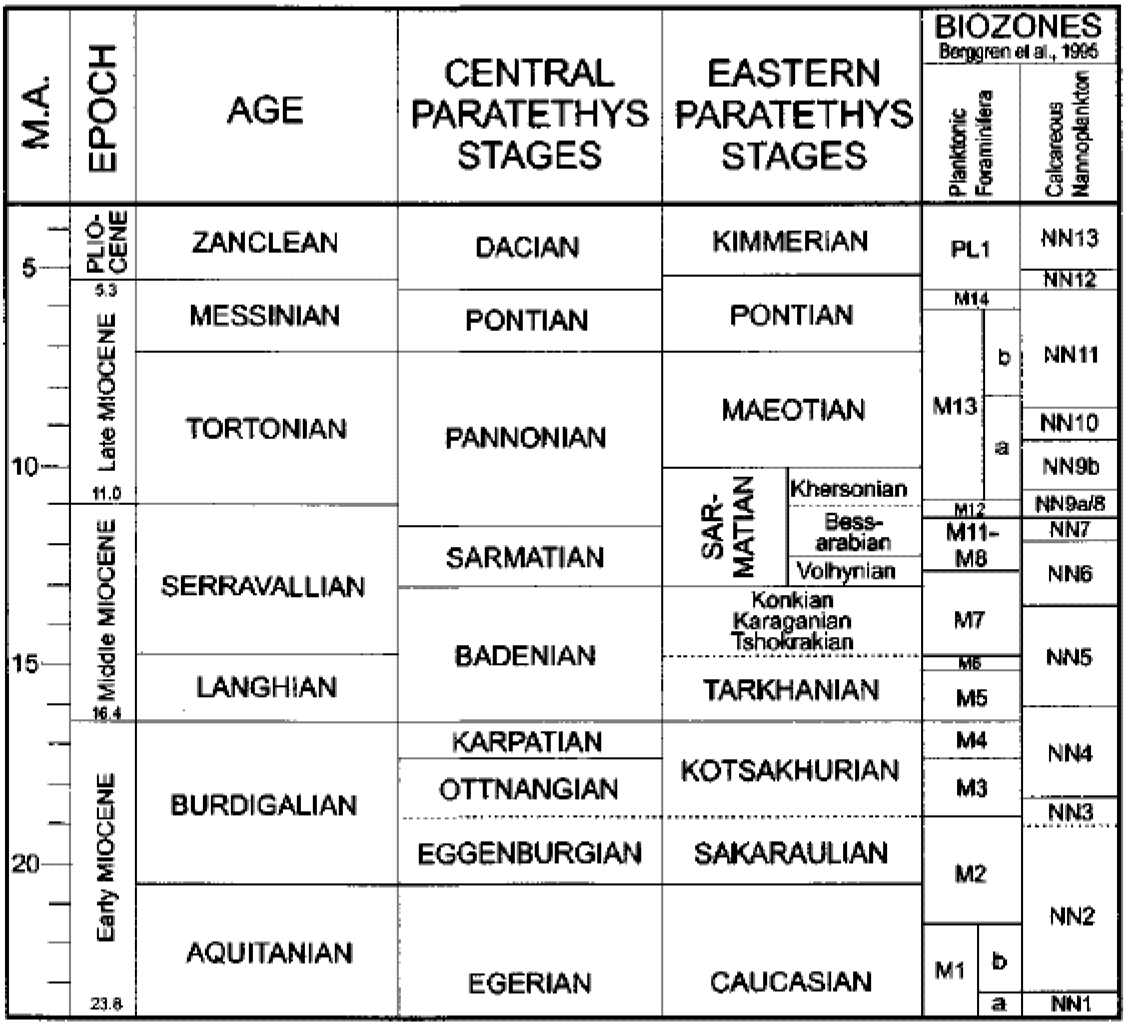

Fig. 2.1, Chronostratigraphy of the Miocene. The pull-apart mechanism started to act in the Karpathian (Piller 1999)

2.3 THE INVESTIGATED SITE; THE MATZEN AREA

The part of Vienna Basin investigated in this thesis is the Matzen area named after the village *Matzen* in its west. It covers an area of approximately 20 x 16 kilometers and is located between the north-west of the city of Vienna and the Slovakian border.

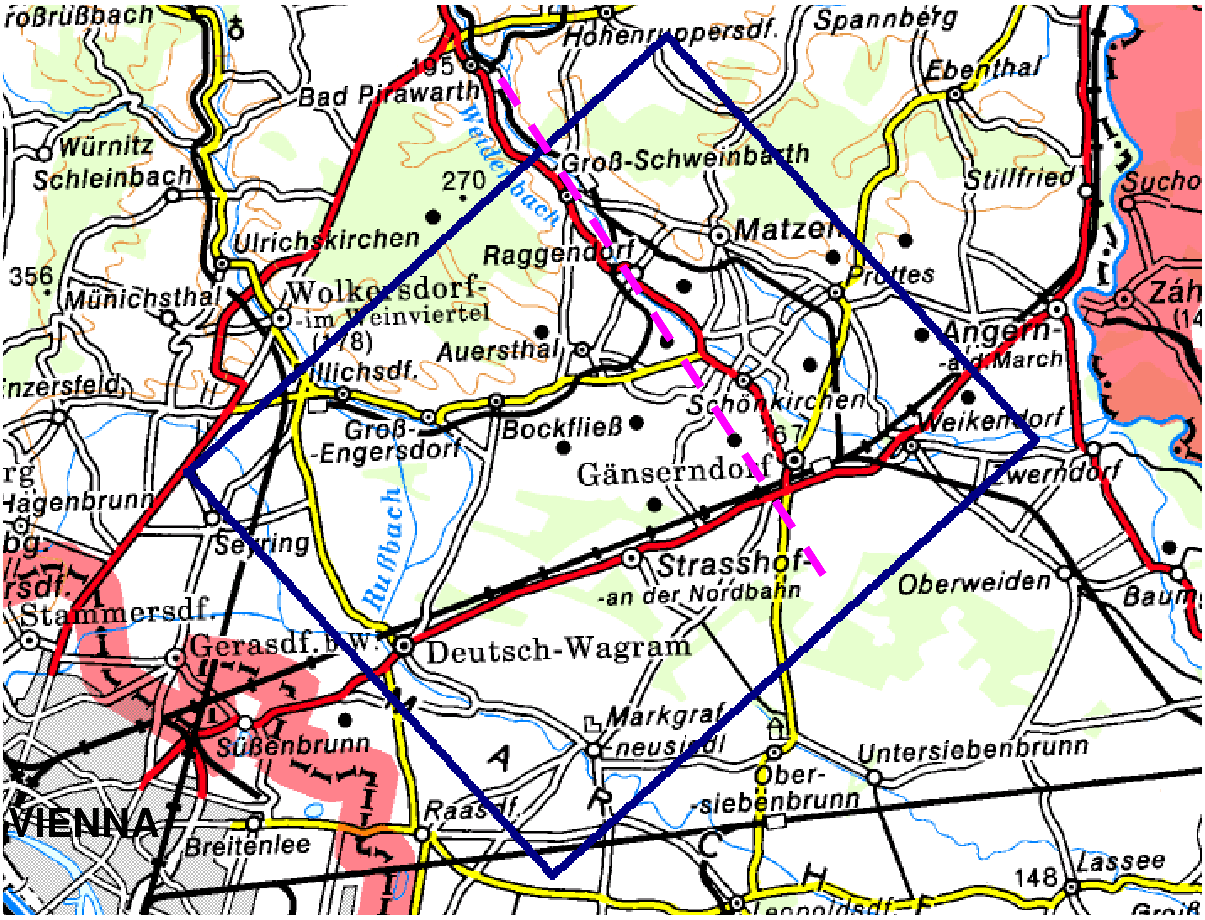

Fig 2.2, map of the Matzen area within the blue rectangle. Black dots are marking the location of exploration and production wells. The pink dotted line represents roughly the location of the vertical 2D cut shown in figure 2.3

The *Northern Calcareous Alps* (see figure 2.4), being one of the most important areas for this thesis, can be subdivided into Frankenfelser Lunzer nappe (Bajuvarikum), the Göller nappe (Tirolikum) and the Higher Calcareous Alps nappe. These nappes are built up primarily of main dolomite and are separated from each other by Gosau layers like the Gießhübler monocline and the Glinzendorfer syncline. (Wessely 1993)

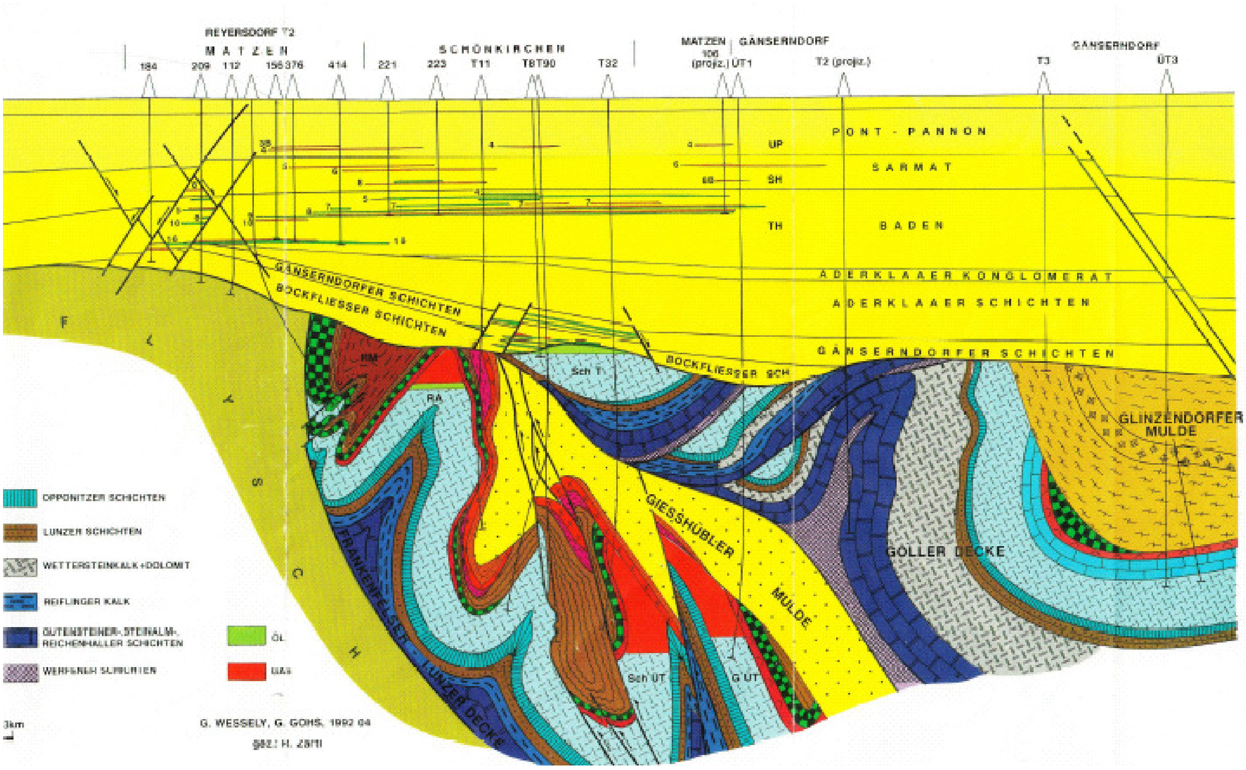

Fig 2.3, Cross section of the Matzen area showing the uppermost Neogene and a rough model of the underlying Northern Calcareous Alps and partly the Flysch zone. The highly folded and overhanging structures between the Frankenfelser-Lunzer nappe and the Gießhübler monocline are supposed to be hydrocarbon reservoirs. (source: Brix/Schultz, 1993, attachment 4)

2.4 HYDROCARBONS

In their book “Erdöl und Erdgas in Österreich” Brix and Schultz (1993) provide a comprehensive overview of hydrocarbon exploration and production in the Vienna Basin.

The appearance of oil and gas in the Vienna Basin has already been know since the 19th century. Commercial exploration and production started in the 1930s, where shallow reservoirs were the first targets. In the 1950’s the giant oil field in the Matzen area was discovered with approximately 80 M tonnes of initial oil reserves. In the 1980’s a drilling depth of more than 8000´s meters was established and hydrocarbon reservoirs were found in all three floors of the basin.

The Matzen oilfield is one of the largest reservoirs in Central Europe. It contains oil and gas in the Neogene Basin fill and in the Calcareous Basin floor as well, reservoir depths are ranging from 500 to 6000 meters. The largest gas deposits were discovered in the *Reyersdorfer dolomite* (RA) and in the *Schönkirchen Tief formation* (Sch T, see figure 2.4). However, further remarkable reservoirs are expected in deeper, overhanging structures of the Frankenfelser-Lunzer nappe. Therefore a deeper understanding of the geological and structural setting in the deep Vienna Basin is one of the future tasks (Brix 1993; Hamilton 1999).

3. SEISMIC VELOCITIES

3.1 THEORY OF WAVE PROPAGATION

Seismic methods utilize the propagation of waves travelling through the earth, which depends on the elastic properties and physical parameters of the rocks in the subsurface. Elastic properties of an acoustic medium can be described as the relation between stress and strain with the generalized form of *Hooke´s law:*

$$\sigma_{ij} = c_{ijkl} \cdot \varepsilon_{kl} \qquad \text{(Eq. 3.1)}$$

σ_{ij}	stress tensor
c_{ijkl}	elastic moduli tensor
ε_{kl}	strain tensor

Eq. 3.1 gets simplified in case of an isotropic medium:

$$\sigma_{ij} = \lambda\theta\delta_{ij} + 2\mu\varepsilon_{ij} \qquad \text{(Eq. 3.2)}$$

θ	cubic dilatation
μ, λ	Lame parameter for isotropic media
δ_{ij}	Kronecker symbol

The law of motion relates displacement to stress:

$$\rho \frac{\partial^2 u_i(x,t)}{\partial t^2} = \frac{\partial \sigma_{ij}(x,t)}{\partial x_j} \qquad \text{(Eq. 3.3)}$$

u	displacement
ρ	density

A combination of *Hooke´s law* and the *law of motion* using the *Helmholtz decomposition* leads to a scalar potential field describing the P-waves (Eq. 3.4a) with velocity α:

$$\nabla^2\phi = \frac{1}{\alpha^2}\frac{\partial^2}{\partial t^2}\phi \qquad \text{(Eq 3.4a)} \qquad \text{where} \qquad \alpha = \sqrt{\frac{\lambda+2\mu}{\rho}} \qquad \text{(Eq. 3.4b)}$$

- and to a vector potential field describing S-waves with their velocity β:

$$\nabla^2\Psi = \frac{1}{\beta^2}\frac{\partial^2}{\partial t^2}\Psi \qquad \text{(Eq 3.5a)} \qquad \text{where} \qquad \beta = \sqrt{\frac{\mu}{\rho}} \qquad \text{(Eq. 3.5b)}$$

Both Eq. 3.4a and Eq. 3.5a are examples of the *wave equation* (Eq 3.6), which gives the relation between the time derivative to spatial derivative of displacement, where V^2 is the constant of proportionality.

$$\frac{1}{V^2}\frac{\partial^2}{\partial t^2}\Theta = \nabla^2\Theta \qquad \text{(Eq. 3.6)}$$

Ray tracing is a widely used method in many fields of seismology for solving the wave equation. It is an approximation that can be easily calculated by computer programs and leads to reliable interpretations. The ray tracing theory is based on the *eiconal equation* (Eq 3.7), which is an approximated solution for the wave equation at high frequencies. *High frequencies* in this context means, that wavelengths are short compared to the gradient of the velocity field. (Aki, Richards 2002, 22f; Lowrie 1997, 120f; Telford 1990, 140f)

$$|\nabla T(x)|^2 = \frac{1}{v(x)^2} \qquad \text{(Eq. 3.7)}$$

T	phase factor
v	velocity

3.2 FACTORS AFFECTING SEISMIC VELOCITY

Experience shows, that seismic velocities increase with depth as consequence of increased pressure in deeper buried layers caused by the load of overlying rocks. As equation 3.4b shows, that the velocity of P waves travelling trough homogeneous elastic media is a function of density ρ and the lame parameters μ and λ. One might expect that the Lame parameters, which are affected mainly by intermolecular forces, are independent on pressure. Due to the fact, that rocks are slightly compressible, density should increase with pressure. Density is the denominator in this expression, hence this would lead to the assumption that increasing depth leads to decreasing seismic velocity, which is contrary to actual observations. The solution to this is that rocks, even if they are considered to be solid and homogeneous, are composed of minerals and have a porous structure, and porosity is the most important factor in determining seismic velocities. Compaction as a consequence of increased pressure results in loss of porosity and furthermore increasing density. Changes in porosity affect the elastic properties of the media significantly, so that lame parameters become governing factors in velocity changes. According to Faust (1953) a rule of thumb (Eq. 3.8) describes the *seismic velocity V* as a function of *burial depth Z* and *formation´s electrical resistivity R*.

$$V = 2000 \times (ZR)^{\frac{1}{6}} \qquad \text{(Eq. 3.8)}$$

Obviously there seems to be an empirical relation between mechanical and electrical properties of rocks. This becomes even clearer if one considers that porosity is also one of the governing factors in determining rock resistivity.

In porous rocks the pores are filled in most cases with fluid media, which can be either water, oil or gas. Due to the fact that oil is slightly more compressible than water, oil filled pores lead to little lower velocity than water filled pores. Gas is much more compressible than water or oil, thus gas filled pores result in much lower seismic velocities than pores filled with oil or water. The fact that seismic velocities depend on the type of the pore fluid can be used as hydrocarbon indicator. Figure 3.1 shows the density-velocity relationship for given lithologies. The overlapping ranges of density and velocity as a consequence of different porosities makes it hardly possible to determine the lithology of a sample only from its P wave velocity.

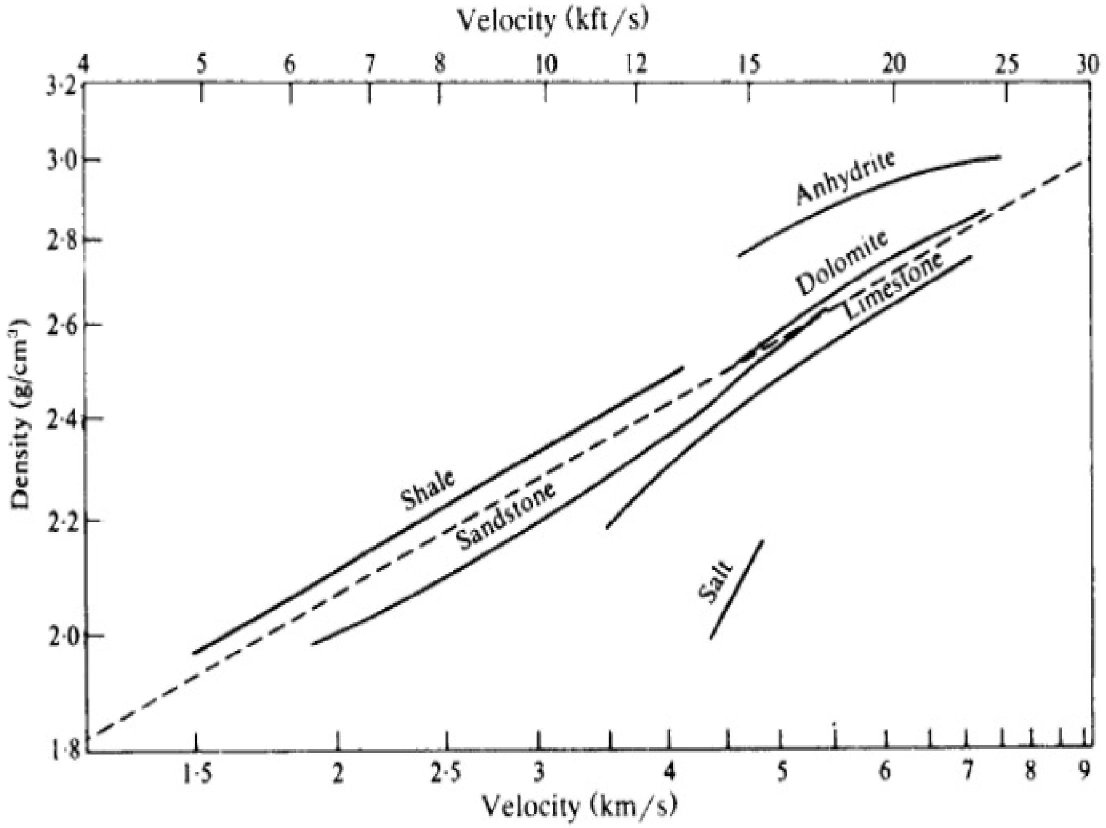

Fig 3.1, Relationship between P wave velocity and density. The wide range of values and the overlap results from of different porosities within the lithologies.

The factor that relates S waves and P waves velocities varies with the type of rock the waves are travelling through and can therefore be used for lithology determination. Furthermore S waves velocity is rather insensitive to the type of fluid the pore space is filled with, whereas P wave velocity depends strongly on the pore fluid. Hence, local changes of S to P wave ratio can be utilized as a hydrocarbon indicator also (Telford 1990, 158ff).

3.3 DEFINITION OF SOME COMMONLY USED VELOCITY TERMS

- INTERVAL VELOCITY

The average velocity of a seismic wave travels through of certain subsurface layer of rock bordered by two reflectors. Typically used is the velocity of P waves, which is assumed to be constant within this certain layer. The interval velocity is commonly determined by acoustic logs or from changes in stacking velocities from different seismic events in common midpoint gathers. Interval velocities can also be derived from RMS velocities using the Dix conversion.

- AVERAGE VELOCITY

The average velocity V_{AVG} can be described as the ratio between the length of a certain ray path and the time it takes the wave to travel along this path. It can be also considered to be the mean value of the interval velocities of the layers the wave traverse along its path (Eq. 3.9). Commonly the ray path is assumed to be perpendicular to the wavefront.

$$V_{AVG} = \frac{\sum V_i . t_i}{\sum t_i} \qquad \text{(Eq. 3.9)}$$

- ROOT-MEAN-SQUARE VELOCITY (RMS)

V_{RMS} is defined as

$$V_{RMS} = \frac{1}{t_0} . \sum_i^1 V_i^2 . t_i \qquad \text{(Eq. 3.10)}$$

- NORMAL-MOVE-OUT VELOCITY (NMO)

The time between a wave is recorded at a given offset x and at the zero offset position is called normal move out time t_N .

$$t_n^2 = t_0^2 + \frac{x^2}{v_n^2} \qquad \text{(Eq. 3.11)}$$

In order to stack all the seismic events that originate from one common reflection point in the subsurface this hyperbolic NMO has to be corrected.

The velocity required for this correction is called NMO velocity v_n, which has the same value as the medium velocity in case of a isotropic horizontally layered earth. For short offsets the NMO velocity can be considered to be equal to the RMS velocity (Eq. 3.10).

- STACKING VELOCITY

The value of the stacking velocity is usually determined by velocity analysis like the constant velocity stack, that is used in a conventional common-midpoint-stacking. In case of zero offset and a horizontally layered subsurface the stacking velocity can be considered to be equal with the NMO velocity.

(Yilmaz 2001, 272 ff; Sherrif 2002, 377 ff)

4 BOREHOLE MEASUREMENTS

All over the Vienna Basin hundreds of boreholes have been drilled within the last century. As a consequence of intense exploration and hydrocarbon production in the investigated area OMV built up a comprehensive borehole data base during the last decades. In order to get a model that represents the actual velocity distribution in the deeper Vienna Basin as accurate as possible, velocity information from a borehole that can be assigned to a certain depth or geological structure, like sonic logs and checkshots, is a valuable input that enhances the reliability of the final product.
To determine the intrinsic attenuation of rock layers along the well path a vertical seismic profiling (VSP) data set was utilized. Of course, because of its one dimensional extension a borehole cannot provide lateral information, therefore a dense distribution of deep reaching boreholes within the area of interest is desirable. Unfortunately only a limited number of wells are reaching the required depth which should be significantly deeper than the bottom of the Neogene basin fill.

4.1 SONIC LOGGING

In order to get a vertical velocity distribution along a well path wireline sonic logging is a commonly used method. In principle a sonic logger consists of a receiver a few meters spaced from a sonic transmitter, that emits acoustic energy to the adjacent rock. The receiver measures the travel time of the first arrival of the P waves, which can be used to calculate the P wave velocity. This provides the opportunity for in situ measurement of the elastic properties with a high vertical resolution, 10 cm spacing between two data points are common. On the other hand, because of the high data point density sudden changes in borehole geometry, lithology, grain size or fractures lead to rather noisy data. In order to supplement seismic sections with borehole data synthetic seismograms, similar to corridor stacks achieved from vertical seismic profiling, can be calculated on sonic logs (Telford 1990, 668f).

	P waves		S waves	
Material	V_P (m/s)	Δt (µs/m)	V_S (m/s)	Δt (µs/m)
Water	1400-1600	714-625		
Salt	4570	219		
Shale	4875	205		
Iron casing	5334	187		
Unconsolidated sand	5180	193		
Sandstone	5490-594	182-168	3550	282
Limestone	6400-7010	156-143	3400	294
Dolomite	7010-7925	143-126	4000	250

Tab. 4.1, Common values of fluid and matrix velocities measured with sonic log.
source: Telford 1990, 668

4.2 VERTICAL SEISMIC PROFILING (VSP)

VSP is a class of borehole seismic method that involves a seismic source and a geophone placed in the borehole that records the travel time of the first arrivals of a seismic wave. The source can be either placed near the well head (zero-offset VSP), away from the well head (offset VSP) or with increasing distance from shot to shot (walk-away-VSP). Commonly used are repeatable sources like airguns blasting into a mudpit or vibrators. The final product of VSP is a corridor stack (fig. 4.1d) that highlights the dominant reflecting horizons to be correlated with geological information and common seismic data. Moreover, VSP data often provides more reliable information on the subsurface around the well path than synthetic seismograms derived from seismic logs. This is due to the bandwidth of the recorded signal, which is closer to seismic data than sonic logs and even more important, VSP is less sensitive on borehole conditions.

The geophone is placed in a certain depth and records the entire wavetrain which consists not only of the direct wave, but also of various multiples and reflections. For reasons of enhanced efficiency commonly several borehole tools with integrated geophones are linked together with a spacing of 10 to 20 meters between them. Usually a various number of wave trains are recorded at the same geophone location in order to enhance the signal to noise ratio. Then the geophone chain is moved to the next position and the recording process starts again. Thus, a repeatable source that ensures a constant wave form is essential for a VSP survey.

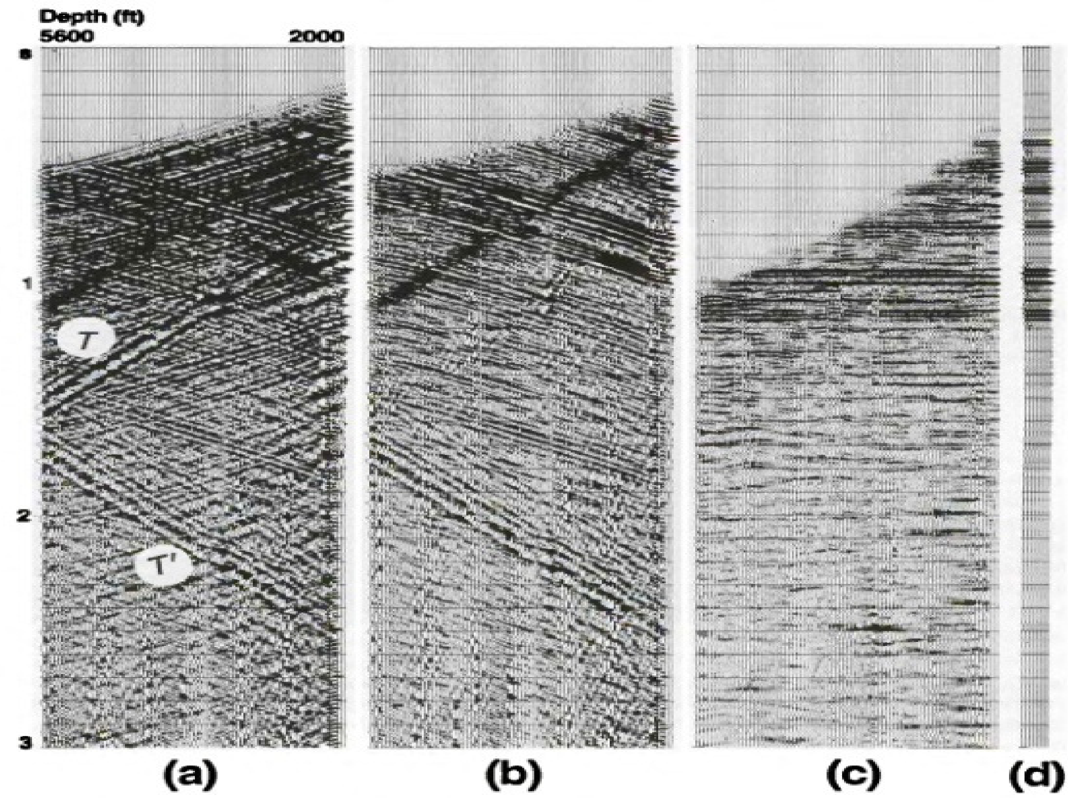

Fig. 4.1, Example of VSP section in different processing stages. (a) raw data, both the upcoming wavefield (right dipping) and the downgoing wavefield can be identified easily. The prominent events T and T' are tube waves travelling through the borehole. (b) upcoming wavefield that comes originates from reflections. (c) upcoming wavefield after static correction and filtering. (d) corridor stack. source: Yilmaz 2001, 1909

A VSP section (example fig. 4.1) consists mainly of the upcoming and the downgoing wave field, which are separated from each other within the first processing steps using for example f-k filtering. The downgoing wave field, which should be mainly the direct wavetrains provide information that is used for deconvolution and on seismic velocities.
The upcoming wavefield, after static correction and filtering, is summed up to obtain a corridor stack, which shows the dominant reflections that can be correlated with geological structures (Yilmaz 2001, 1907f, Telford 1990, 668)

4.3 CHECKSHOTS

If not a full VSP section with all the dominant reflectors, but an overall information on velocity and travel time along the wellpath or within a certain formation is the task, a checkshot survey might be an alternative to a full VSP survey. To determine the time a wavelet travels through the subsurface to a certain depth a geophone is lowered into the borehole to the depth of interest. A seismic source located close to the well head initiates a wavelet in the subsurface. The receiver, encountering the first arrival of energy, records the travel time of the seismic wave. Assuming a close to vertical raypath the average velocity can be computed easily. In contrast to VSP a checkshot survey uses less and irregularly spaced geophone positions. Since a checkshot survey yields a directly measured relation between depth and travel time of the first arrival, data is considered to be qualified and reliable. P wave velocities derived from checkshot data of several deep reaching boreholes are one of the most important inputs for setting up a velocity model for the deep Vienna Basin (Schlumberger Ltd. 2012).

5 MIGRATION, PRINCIPLES AND METHODS

Migration in seismic data processing itself can be described as an inversion operation that rearranges seismic data elements in a way that seismic events can be plotted in their correct position in the subsurface. Reflections and diffractions in an unmigrated section do not appear at their correct location in the subsurface as a consequence of dipping horizons and variable seismic velocities. Migration now is the process that moves reflections from dipping horizons to their true subsurface position and that collapses diffraction on a seismic section in order to enhance the spatial resolution of the image

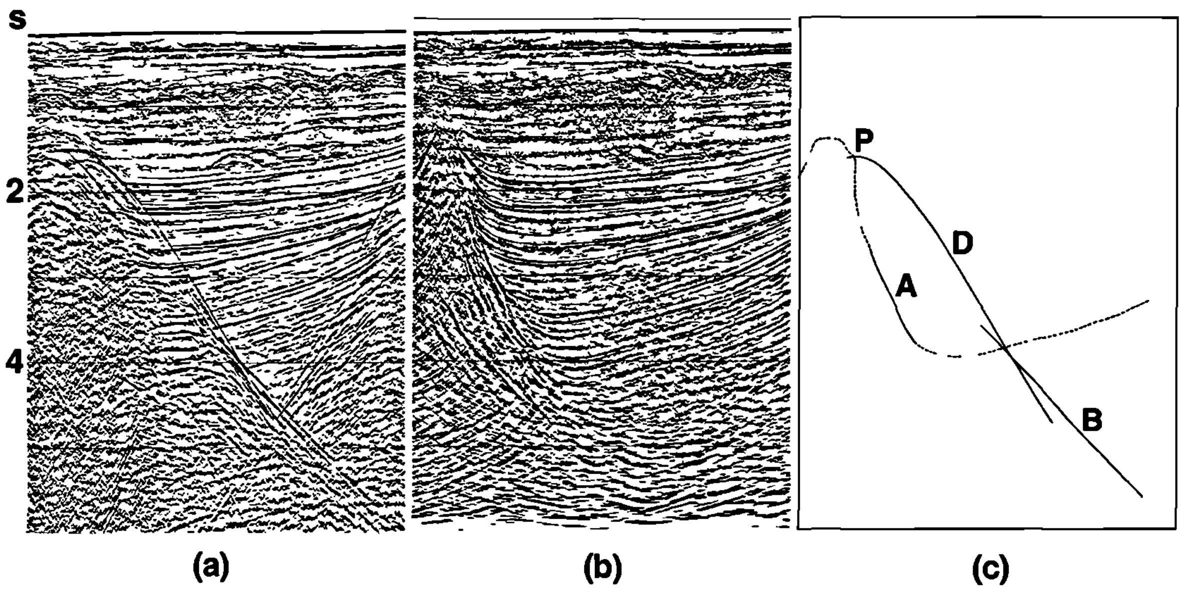

Fig. 5.1, CMP stack of a salt dome structure before (a) and after (b) migration. (c) shows a sketch of prominent dipping events and diffractions in both (a) and (b).
source: Yilmaz, 2001,Vol.1,463

Figure 5.1 shows a stacked section of salt dome structure which is flanked by a slightly dipping strata. Image (c) sketches the prominent seismic events, in which D represents the diffraction hyperbola that originates on the top of the salt dome, whereas B can be associated to the flank of the salt dome in the unmigrated section (a).
After the migration process the diffraction D got collapsed to its apex P and reflection B moved to position A. In contrary the gently dipping strata only moved a little (*Yilmaz, 2001,Vol.1,463ff*; .*Sheriff, 2002, 232f*).

5.1 TIME MIGRATION VS. DEPTH MIGRATION

Most of the migrated sections are displayed having their vertical z-axis in time domain. One reason for this is that seismic raw data in general is recorded in time. To make migrated and unmigrated seismic section comparable, imaging both data sets having their z-axis in time domain is preferred. Another reason for this might be that for depth calculation an accurate velocity model of the subsurface is needed, but velocity estimation based on seismic data often does not meet these requirements. Therefore depth conversion is not necessarily accurate. The process which produces a migrated section in time domain is called *time migration*. This is the way to choose when lateral velocity variations are assumed to be small to moderate.

Strong lateral velocity variation caused by complex geological structures (like imbricate structures caused by overthrust tectonics or salt diapirs) or simply facies changes require imaging in depth domain. This becomes more important, when illuminating of reflection horizons beneath lateral bordered high velocity zones such as salt diapirs is the task. Of course this requires a sufficiently accurate velocity model. Figure 5.2, shows the different results of time and depth migration applied to an artificial model of a salt dome structure. In both cases the same accurate velocity model was used. The top of the salt diapir is imaged correctly in time and in depth migration as well, but seismic events underneath the high velocity zone corresponding to the salt diapir are not displayed correctly and look distorted after time migration.

In contrary depth migration yields a proper image of the given model. This is because lateral velocity inhomogeneities are not considered in time migration (Yilmaz 2001, Vol.1& 2).

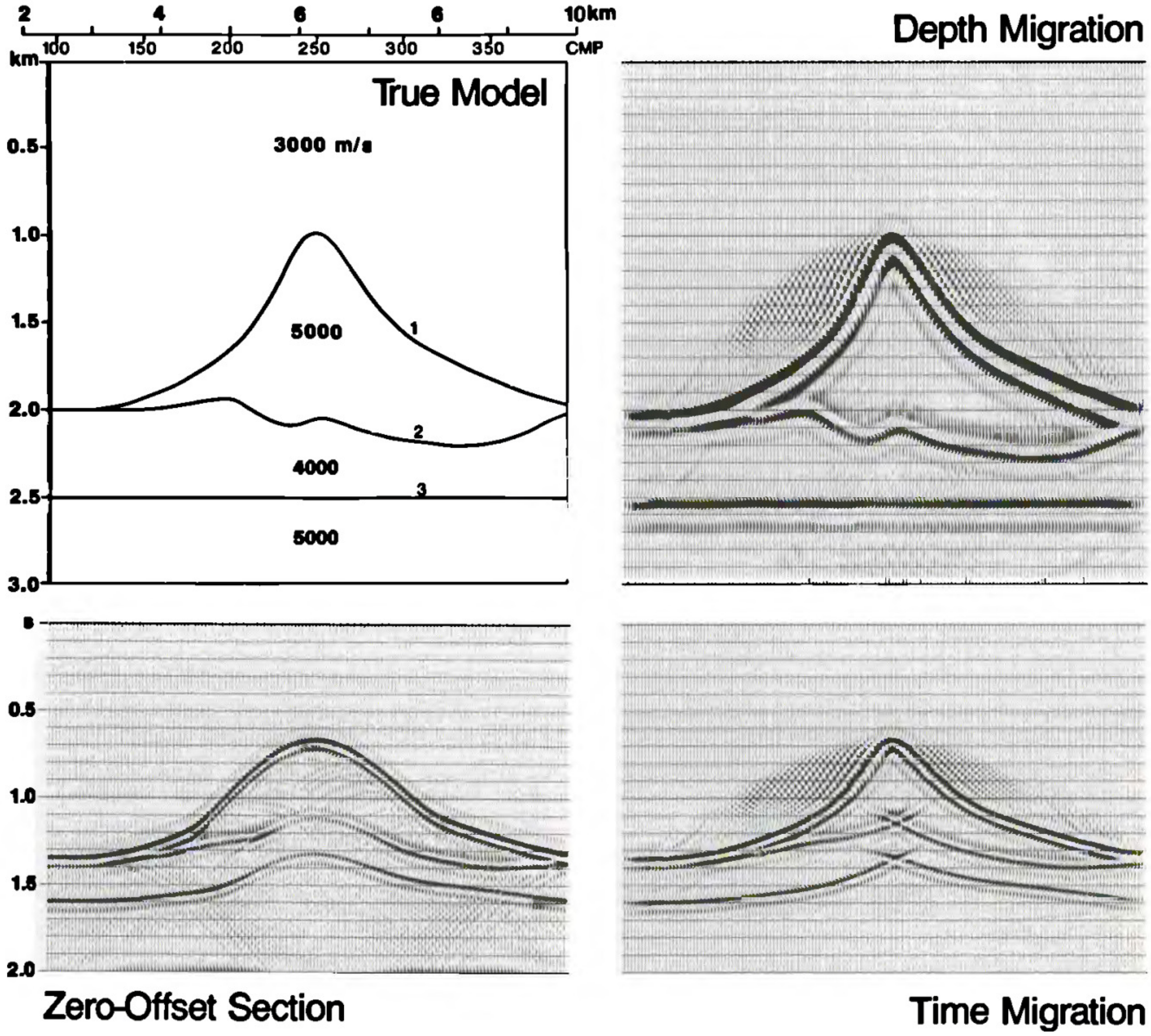

Fig. 5.2, Time and depth migration of the zero offset section associated with an artificial salt diapir model. source: Yilmaz 2001, 1245f

5.2 3D PRE STACK DEPTH MIGRATION (3D-PSDM)

A complete 3D PSDM seismic section of our area of interest and the associated 3D velocity field are one of the main data inputs for this thesis. Hence, it is worth taking a quick overview to PSDM technique and its advantages.

The principle of post stack migration is, that the migration is applied to the seismic section after stacking seismic traces. The main reason of so called CMP stacking (common mid point stacking) is to obtain a *zero offset section*, which should fairly represent seismic waves taking a vertical raypath from source to receiver. One of the advantages of post stack migration, either time or depth migration, is that it is “cheaper” in terms of computing time. Therefore in times of limited computer performance post stack migration was the preferred method. And of course stacking traces improves the signal-to-noise ratio significantly.

What are the main reasons for performing a 3D PSDM? As mentioned in the previous chapter significant changes in lateral seismic velocity distribution are the reason why seismic reflection recorded at the same time to not origin necessarily from the same depth. This makes *depth migration* essential. Furthermore before stacking traces a so called *normal moveout correction* (NMO), which eliminates hyperbolic moveouts in seismic traces, has to be done. When lateral velocity inhomogeneities are not negligible, moveouts are not strictly hyperbolic any more. In order to account for this non-hyperbolic moveouts migration has to be performed before stacking. And finally, the reason for doing this in three dimensions is to account for complex geological structures causing these lateral variations.

Following Yilmaz this can be shortly concluded as*: “In a strict theoretical sense, in the presence of lateral velocity variations, you need to image the subsurface by migration of seismic data in depth, before stack and in three dimensions”* (Yilmaz, 2001, 1321)

5.3 COMMON REFLECTION SURFACE STACK (CRS)

The quality of seismic sections being imaged with conventional data processing methods like NMO/DMO stack or Pre-stack-migration depends largely on the accuracy of the velocity model being used. A common-reflection-surface stack provides a zero offset section from seismic multicoverage reflection data without the need of an accurate macrovelocity model. The transformation from reflection data to a zero offset stack is based on a spatial stacking operator, which is completely data derived and therefore independent on kinematic parameters like a velocity model.

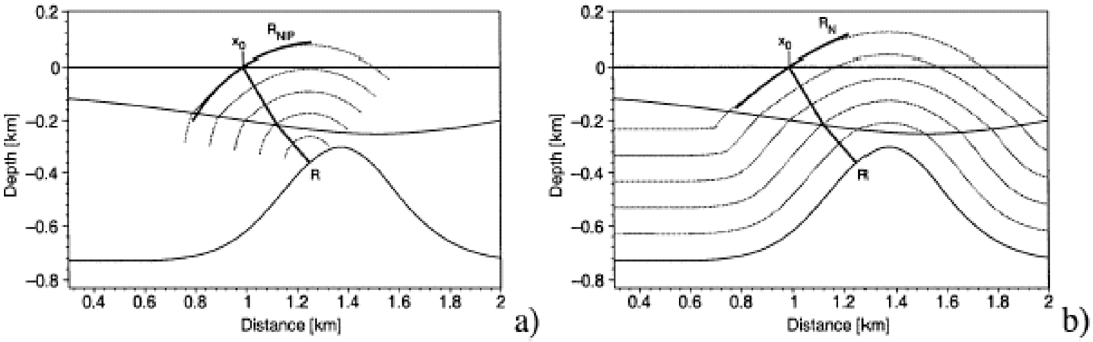

Fig. 5.3, (a) NIP wave for a point source at R, (b) normal wave N for the exploding reflector at R. The wavefronts are displayed as if the uppermost layer would extend above the seismic line. source: Jäger et al 2001

This CRS stacking operator can be derived from three wavefront attributes of two so called eigenwaves, which are part of a hypothetical experiment illustrated in figure 5.3.

- R_{NIP}, radius of the normal incidence wave (NIP) originating from a point source in R
- RN, radius of the normal wave originating from an exploding reflector in R
- α, emergence angle of the zero offset ray

This parameter triplet needs to be calculated for every single point of the zero offset section by analyzing the primary reflections. This problem is addressed with various optimization algorithms. The only model parameter required is the near surface velocity (Jaeger et al 2001).

6. ATTENUATION OF SEISMIC WAVES

As they are travelling through acoustic media seismic waves are facing a continuous decay of their amplitude. Several physical effects are the main reasons for decrease of energy.

- Spherical divergence
- Partitioning of energy at interfaces
- Absorption

6.1 SPHERICAL DIVERGENCE

Note: the following considerations hold for body waves, but not for surface waves

The most important reduction of amplitude is caused by geometrical effects. Seismic energy that propagates through an isotropic media creates a spherical wave front. The energy of the wave originating hypothetically from one single point is distributed continuously over the spherical surface of the wave.

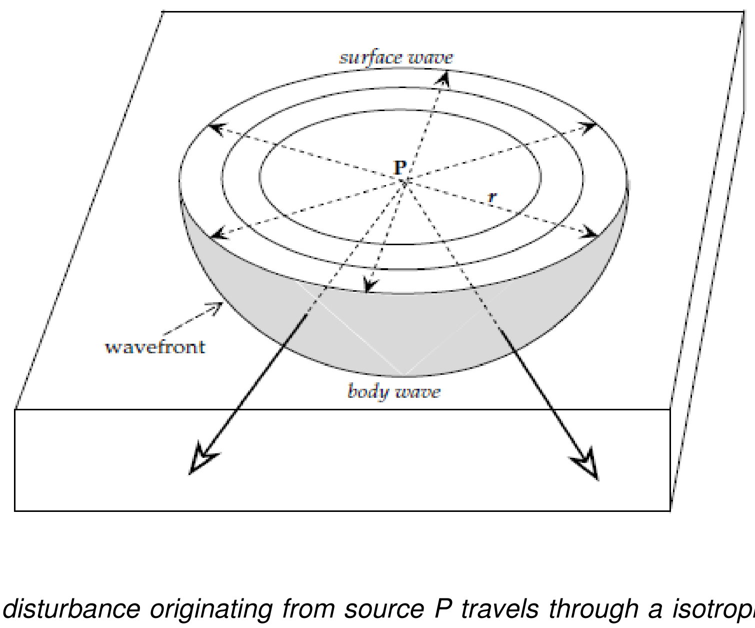

Fig 6.1, A seismic disturbance originating from source P travels through a isotropic homogenous half space. The wave front of the body waves in the subsurface occurs as half sphere, the amplitude decreases inversely to the distance from P. source: Lowrie, 1997, 130

As the surface of a sphere increases proportionally as the square of its radius, the energy per unit area decays inversely as the square of the distance from the source as a consequence of geometrical spreading. The damping of the seismic wave is quantified by its affect on the amplitude recorded by the geophones. The relationship between energy density and amplitude of a harmonic wave is given with Eq. 6.1.

$$\mathrm{E} = \frac{\rho\omega^2 \mathrm{A}^2}{2} \qquad \text{(Eq. 6.1)}$$

Thus, the energy density E is proportional to the square of amplitude A of the seismic disturbance, therefore the amplitude decrease inversely to the distance from the source. Considering only a small section of the sphere in great distance from its point of origin the wave front can be considered to be plane and geometrical effects become negligible. The effect of spherical divergence of a wavelet´s A amplitude at distances x and x_0 is given with Eq.6.2.

$$A(x) = A(x_0).\left(\frac{x_0}{x}\right)^n \qquad \text{(Eq. 6.2)}$$

The exponent n depends on the geometry of the wave propagation. For a plane wave n becomes zero, for a spherical wave *n = 1* (Schön, 1996, 283f).

6.2 PARTITIONING OF ENERGY AT INTERFACES

In seismics different layers in the subsurface are distinguished by their elastic properties, namely by their acoustic impedance Z_i, which is nothing but the product of its P-wave velocity α_i and its density ρ_i. As a seismic wave crosses the interfaces between two lithological units characterized by an impedance contrast it gets separated into its reflected and its refracted part. Assuming a plane wave front the amplitude A_i and angle θ_i of reflected and refracted energy are determined by Snell's law and the Zoeprittz equations. Solving the simplified forms of the Zoeprittz equations valid for normal incidence (Eq. 6.2) gives the transmission coefficient T and the reflection coefficient R, which determine the amplitude of the transmitted and reflected wave (Lowrie 1997; Telford 1990).

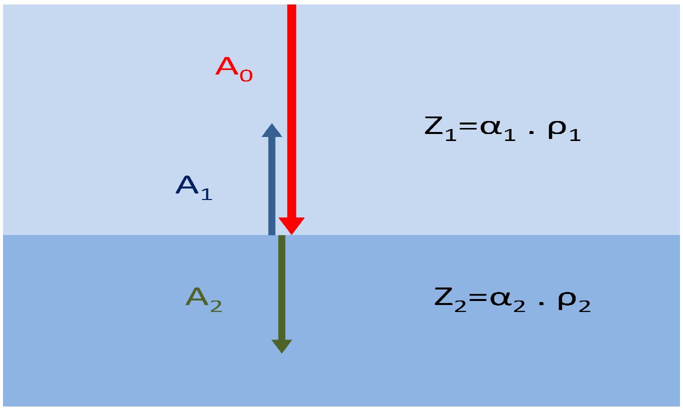

Fig 6.2, Boundaries between two layers of different acoustic impedance Z determined by its seismic velocity α and density ρ. Assuming a plane wave front and vertical incidence the amplitude of the incident (A0), reflected (A1) and transmitted (A2) are given by Eq. 6.2

$$A_1 + A_2 = A_0 \qquad Z_1A1 - Z_2A_2 = -Z_1A_0$$

$$R = \frac{A_1}{A_2} = \frac{Z_2 - Z_1}{Z_1 + Z_2} \qquad T = \frac{A_2}{A_2} = \frac{2Z_1}{Z_1 + Z_2} \qquad \text{(Eq. 6.2)}$$

6.3 ABSORPTION

An acoustic medium never has perfect elastic properties. The energy associated with the seismic wave is always absorbed gradually by the medium and gets transformed into heat as a consequence of imperfect elastic reaction of particles with their neighbors. This effect is called *anelastic damping, intrinsic attenuation* or *absorption* and is a highly variable property of rock material that depends on many parameters e.g. confining pressure, porosity, type and temperature of pore fluid etc. In general attenuation decreases with increasing depth and rock cementation, but increases with porosity.

Many mechanisms are involved into absorption like piezoelectric and thermoelectric effects or viscous losses of pore fluids. Though some of them are not completely understood yet, the major part of energy loss due absorption can be explained by the friction between particles affected and displaced by a seismic wave passing through.

The rate of damping of the amplitude is quantified by the so called *seismic quality factor Q* which is defined as the ratio between the energy loss ΔE and the total elastic energy E of the wave within one complete harmonic cycle.

$$\frac{1}{Q} = -\frac{\Delta E}{2\pi E} \qquad \text{(Eq. 6.3)}$$

Due to the wave's propagation over a certain distance while facing a loss of energy, a periodic cycle can be associated with the wave length λ. Therefore we can rewrite Eq. 6.3 to

$$\frac{2\pi}{Q} = -\frac{\lambda}{E}\frac{dE}{dr} \quad \rightarrow \quad \frac{dE}{E} = -\frac{2\pi dr}{Q\,\lambda} \qquad \text{(Eq. 6.4)}$$

Following Eq. 6.1 there is a square relationship between energy and amplitude. Substituting and solving Eq. 6.4 gives the attenuated amplitude A measured at distance r from the source location.

$$A = A_0\, exp\left(-\frac{\pi}{Q}\frac{r}{\lambda}\right) \qquad \text{(Eq. 6.5)}$$

As it can be seen easily, the attenuation of the amplitude is governed by the quality factor Q and the wave length. Hence, higher frequencies are facing a higher attenuation than the lower ones. The relationship between a signal's damping and its frequency content establishes the basis of the spectral ratio method to determine the Q factors from VSP data.

Another commonly used term to quantify the intrinsic attenuation of rock material is the frequency dependent absorption coefficient α. Applying this relation Eq. 6.4 gets simplified to:

$$A = A_0 e^{-r\alpha} \qquad \text{with} \qquad \alpha = \frac{\pi}{Q.\lambda} \qquad \text{(Eq. 6.6)}$$

(Aki, Richards 2002, Schön 1996; Lowrie 1997; Stainsby et al 1985)

6.4 METHODS OF SEISMIC QUALITY FACTOR DETERMINATION

To determine the Q value based on VSP data a number of different methods can be used. According to Tonn (1991) this methods can be separated into two different general approaches, those using time domain and those using frequency domain.
The most important methods will be briefly highlighted in the following.

a) Time domain methods

Amplitude decay method: This the simplest form of Q factor determination. The ratio of the wavelet's amplitude at two different distances or travel times is used compute the Q factor. This method respects only the dominant frequency and requires of course true amplitude recordings.

Wavelet modeling: This method utilizes a reference wavelet recorded at a certain depth x_1, which is modeled synthetically with respect to the dispersion relation. The artificial wavelet is modified by varying the Q value until comparison with the actually observed wavelet at a certain depth x_2 yields the best correlation. The comparison is performed by using either the difference of the amplitudes (L1 norm) or the difference of the squares of the amplitudes (L2 norm). Obviously the L2 norm gives more weight to higher amplitudes.

Phase and frequency modeling: Analogous to the previous method phase modeling modifies the instantaneous phases of a wavelet by varying the Q value and applying the dispersion relation. Subsequent comparison with actually observed phases of the wavelet leads to the best fitting results. As the instantaneous frequency is defined as derivative of the instantaneous phase, frequency modeling can be performed easily within this process. Due to the fact that higher frequencies are affected stronger by absorption and the frequency modeling method is more sensitive to higher frequencies, it should be more sensitive to Q factor variations.

Rise time method: A wavelet as it travels through elastic media gets affected by dispersion. According to Gladwin and Stacey (1974) there is an empirical relationship between the rise time of and signal and attenuation, which can be utilized to obtain the Q factor.

b) Frequency domain methods

Using modern computer techniques to compute frequency spectra on time series based data is a task that can be done easily. Numerical software products that are suitable for time series processing are using the *Fast Fourier Transformation (FFT)* to compute the frequency content and amplitude spectra of time series.

Spectral modeling: Analogous to the wavelet modeling approach described above the spectral modeling method utilizes the amplitude spectrum of a reference wavelet to compute synthetically attenuated spectra related to a certain depth by varying the quality factors. Comparison with amplitude spectra of actually recorded wavelets and iterative improvement leads to best approximation.

Spectral ratio method: The amplitude spectra of a reference wavelet and of a wavelet originating from a certain depth are calculated using a Fast Fourier Transform algorithm. As the amplitude decays exponentially in relation to the wavelength according to equation 6.4, the logarithmic ratio of these two amplitude spectra with respect to the frequency yields a linear increase assuming an ideal case. The slope of the straight line is directly proportional to the quality factor Q.

Both spectral modeling and the spectral ratio method are widely used to derive reliable information on intrinsic damping and Q values derived from VSP data. Thus these two approaches are the methods of choice in this thesis and are therefore explained more detailed in chapter 10 (Tonn 1991).

7 AVAILABLE DATA AND TOOLS

To set up the comprehensive model various types of data and state-of-the-art software tools have been provided by OMV. These will be described briefly in the following.

7.1 BORHOLE DATA

Although dozens of boreholes have been drilled in the area of interest during the last decades, not many of them provide utilizable information for this study´s purposes. One of the most important demands on boreholes to be used in this study is that they have to be drilled down to a certain depth. At least they have to reach the section underneath the Neogene Basin floor to provide a significant amount of data of the Calcareous Alps. Wells listed below meet this strict requirement:

Strasshof T001, T002, T004, T005 and T006
Gaenserndorf UBERTIEF 003a
Ebenthal TIEF 001
Schoenkirchen TIEF 001

Corresponding borehole data contains following information:

- P wave velocities coming from sonic log measurements with a very high vertical resolution of 10 to 20 cm.
- Average and interval velocities recorded within a checkshot survey. Since checkshot velocities are the only directly measured time-depth-relation available, they are considered to be qualified data.
- Tops and bottoms of geological units along the well path. Facies changes and geological boundaries are not necessarily coincident with seismic reflectors.

All borehole data is related to the seismic reference datum of 130 meters amsl.

7.2 3D VELOCITY DATA

Two different sets of 3D-seismic velocity data in depth domain have been provided by OMV derived from 3D seismic sections. The BIN size of both data sets is 50m x 50 m with an vertical resolution of 4 meters.

- CRS velocity field
- PSDM velocity field

In order to find out which shows the best fit with check shot data and known geological structures, velocity data of both data sets has been extracted along a well path with significant drilling depth and compared with the velocities achieved from the check shot data of the well. Comparison has been done with average (Fig 7.1a) and interval velocities (Fig 7.1b). Since checkshot data from borehole STRASSHOF T004 is the one with the highest density of data points and even more important it reaches a significant depth of more than 5000 meters this well was chosen for comparison.

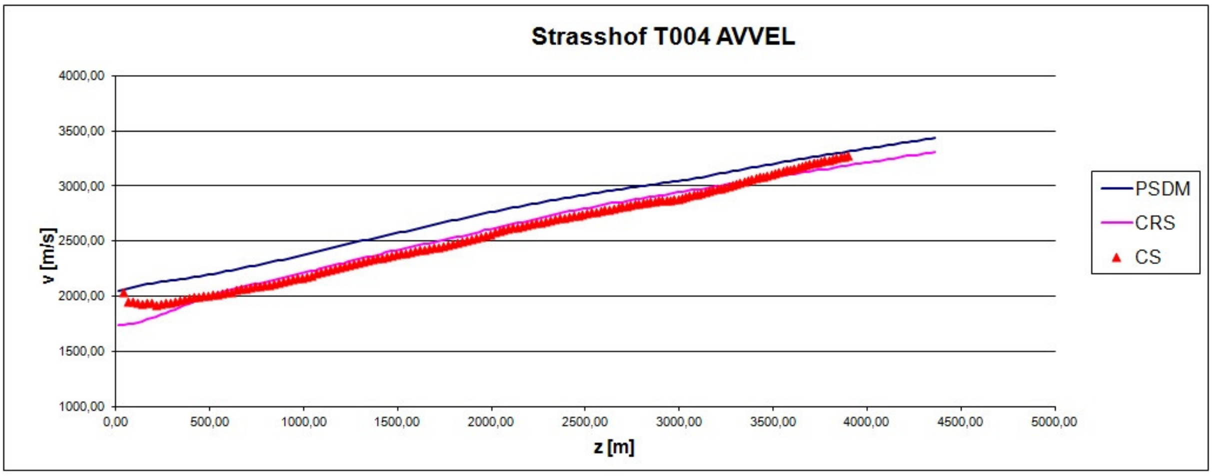

Fig 7.1a, Comparison of average velocities of well Strasshof Tief 004.

Compared to velocities originating from checkshots (CS) the velocities derived from PSDM data seems to be slightly overestimated, whereas CRS velocities show pretty good correlation (see figure 7.1a)

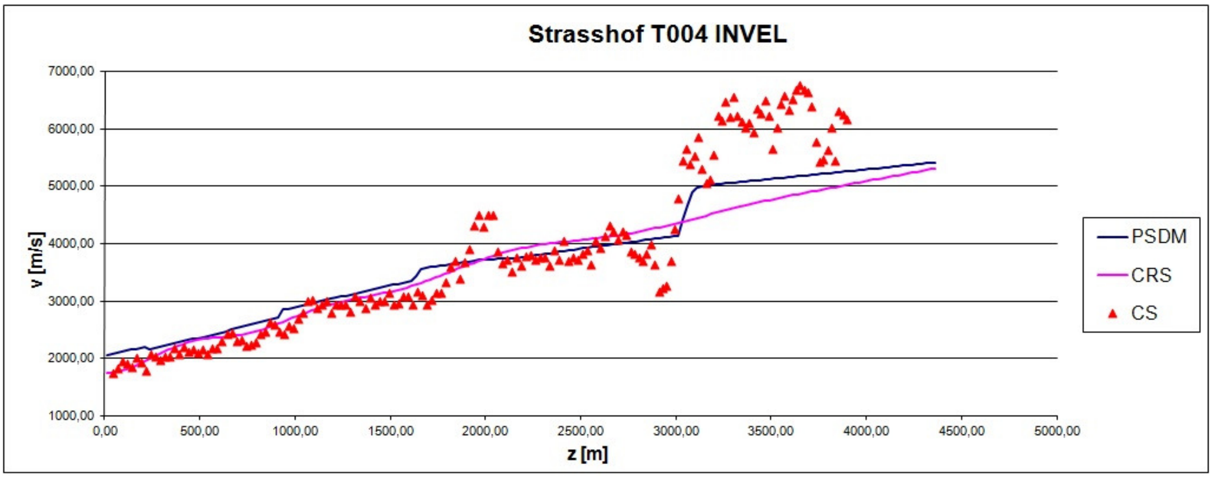

Fig 7.1b Comparison of interval velocities of well Strasshof Tief 004.

Comparing interval velocities depicted in figure 7.1b illustrates, that CRS derived velocities show rather smooth characteristics. In contrast to that PSDM data show sudden increases of velocities that can be assigned facies changes. This is also evident in the checkshot velocities, the significant discontinuity at a depth of approximately 3100 meters can be related to the boundary between the Neogene sediments and the underlying Northern Calcareous Alps.

7.3 HORIZONS AND SEISMIC DATA

As already mentioned in chapter 2 the subsurface structure of the investigated area can be divided into the major lithological blocks according to the rough model given by Wessely (1993). The extension and boundaries of these units are not defined exactly, especially in the deeper section of the Calcareous Alps one has to deal with significant uncertainties. Hence, selected horizons or surfaces have to be extended and their continuation has to be estimated to establish the shape and extension of geological structures bounded by these horizons. The used horizons can be divided into given horizons, estimated horizons and auxiliary horizons. Given horizons like the “Sandschallerzone” have been interpreted on 3D PSDM seismic data set, estimated horizons like the base of Northern Calcareous Alps are horizons based on OMV expert knowledge and the geological map shown in Fig. 2.3 and roughly estimated and interpreted on seismic sections.

Auxiliary horizons do not have any geological relevance, these horizons are only used to distinguish between areas of different interval velocity gradients during the velocity model setup and are not presented in the final structural model. The Z-value of all horizons is given in time domain, zero time is linked to seismic reference datum.

File names of given Horizons of the Neogene section:

PSDM_2MP_smooth_Matzen_Hohenau_Vienna_basin_new, (middle Pannonian)
PSDM_5UP_smooth_Matzen_Hohenau_Vienna_basin_new, (lower Pannonian)
PSDM_lower_sarmathian_smooth_Matzen_Hohenau_Vienna_basin_new (Sarmathian)
Sandschallerzone_smooth_Matzen_Hohenau_Vienna_basin_new (Sandschaller zone)
PSDM_BASIN_FLOOR_smooth_Matzen_Hohenau_Vienna_basin_new (Neogene basin floor)

File names of given horizons of the Northern Calcareous Alps:

REYERSDORFER_DOLOMIT_TIME (Reyersdorfer main dolomite)
SCHOENK_PROTTES_TD_TIME_PS_VIENNA_BASIN (Schönkirchen Tief formation)
GOELLER_THRUST_PS_1_TIME_PS_AA_PS_SEYMATZDCH1 (basement Goeller nappe)

A 3D PSDM seismic section in time domain has been utilized to map the estimated and auxiliary horizons or surfaces. The complete data set covers has an areal extension of approximately 1000 km^2 and covers a large parts of the northern Vienna Basin. In order to keep the file size low it has been cropped to approximately 320 km^2, which still sufficiently covers the area of interest. Of course the 3D velocity data has been cropped to the same size. The inline and crossline spacing is 25 meters, maximum recording time is 4 seconds with an sampling interval of 0.4 milliseconds.

7.4 VSP DATA

To evaluate the intrinsic attenuation of the deep Vienna Basin a set of zero-offset VSP data has been used. For Q value analysis the VSP raw stacks of borehole Strasshof T004 and Strasshof T006 provide proper information in commonly used SEGY file format. Previously performed processing of VSP data sets removed multiple reflections and the upcoming wavefield. In order to enhance the signal-to-noise ratio the records of five to ten shots have been stacked to one seismic trace.

Four VSP geophone shuttles linked together with a fixed spacing of 25 meters have been lowered down to a defined depth and encountered for the first arrival of a wavelet initiated by an airgun blasting into a mudpit working as a seismic source. The record of each geophone is assigned to one seismic trace. Maximum recording time is 5 seconds with a sampling interval of 1 millisecond.

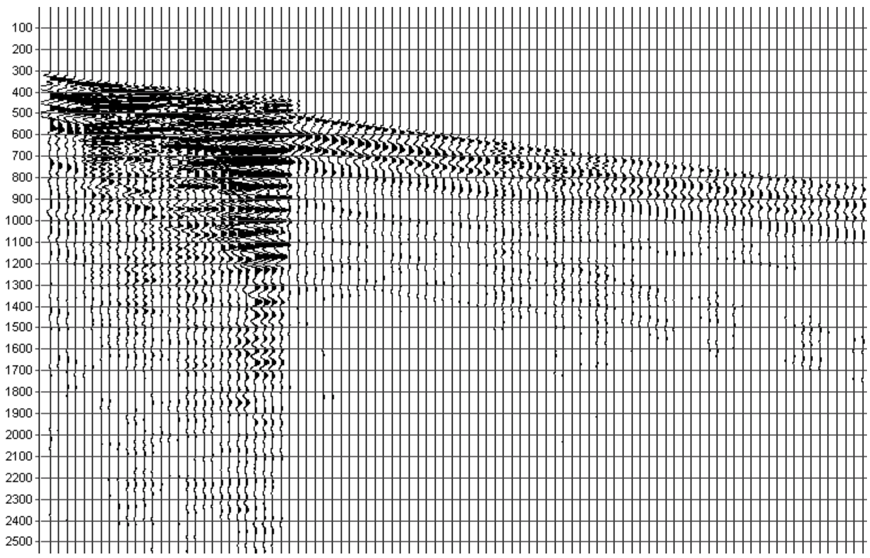

Fig 7.3, Example of a VSP raw stack of the down going wave field of Strasshof T004 used for Q-value determination. Spacing between two traces is 25 meters. The scattered traces on the right side are a result of reverberation of the iron casing of the borehole, these traces can´t be used for further data analysis and have to be deleted.

7.5 SOFTWARE TOOLS

PETREL 2009 , developed by Schlumberger Ltd, is a comprehensive software package for seismic interpretation, geological modeling and reservoir engineering and is widely used in oil and gas industries. Within this study Petrel 2009 has been used for interpreting and mapping of horizons and surfaces, time-depth conversions and setting up the final model containing the demanded information.

MATLAB 2008 was designed by MathWorks Inc. for any kind of matrix calculation and is therefore suitable to deal with data available in tables or matrix format. The opportunity to write small programs or scripts and the use of already implemented functions like the *Fast Fourier Transformation (FFT*) makes MatLab an appropriate tool for time series analysis. Moreover, various software packages for special applications are available for free download in the world wide web. One of these packages is *SeisLab* which offers the opportunity to read file formats used in Oil and Gas Industry and. Reading and analyzing VSP data in SEGY format, calculating of amplitude spectra and Q values and creating the attenuation model has been performed with MatLab

OMNI 3D by GEDCO is seismic acquisition survey design software. Although not used in this study, the final comprehensive model will be the main data input for designing the target oriented survey, therefore the results of this work have to fulfill the requirements of OMNI 3D. All files have to be in ASCII format, velocity information is required in time domain, structural information and surface have to be in depth domain.

8 MODELLING OF STRUCTURAL INFORMATION

8.1 PREREQUISITS ON THE STRUCTURAL MODEL

Following the arrangement of the Vienna Basin suggested in literature (Wessely 1993), the structural model will also consist of two main parts. The upper part encompasses the Neogene and is structured by seismic horizons derived from PSDM seismic data set. The lower part represents the underlying Northern Calcareous Alps and is built with a combination of given horizons and estimated horizons.

Setting up a model starts with nothing but a void space which defines the three-dimensional extensions of the area of interest that needs to be filled with information required to design a seismic acquisition survey. Implementing structural information on geological formations is necessary for two main reasons. Firstly, the target oriented seismic acquisition survey design will be performed later on using the software tool OMNI 3D that uses the ray tracing method amongst others. This requires accurate information on reflecting and refracting boundaries within the model, which is given by various surfaces that separate prominent geological formations from each other. And secondly, in the final model the major geological formations in the Calcareous Alps are characterized by different seismic velocities. When setting up the velocity model with PETREL 2009, seismic horizons are necessary information to distinguish between areas of different seismic velocities respectively different velocity increases.

Before setting up the model some data preparation has to be done. PETREL 2009 distinguishes between *horizons* and *surfaces*. A horizon is a set of single points defined by their coordinates that have been picked along seismic reflectors on inlines and crosslines of 3D sections. By interpolating between these single points using a moving average algorithm a closed surface can be created. Surfaces are needed in PETREL 2009 for model building and time to depth conversion.

The geometrical data has been taken from the PSDM velocity field to make sure, that the surfaces cover exactly the same area as the velocity field. Only the grid resolution of the surfaces has been decreased from 50 meters up to 200 metres in order to keep the file size low but still ensure a sufficiently high resolution.

Horizons and therefore also surfaces are given in time domain as they have been mapped on seismic section given in time domain also. OMNI 3D requires surfaces in depth domain, thus all surfaces of the final structural model have to be converted from time to depth in PETREL 2009 using the PSDM average velocity field.

8.2 SURFACES OF THE NEOGENE BASIN FILL

The Neogene Basin within the area of interest encompasses approximately 3000 vertical meters of tertiary sedimentary strata, which got extensively investigated during hydrocarbon exploration during the last decades. Geological sequences and boundaries are well known and correlate sufficiently with seismic horizons. In order to set up the structural model of the Neogene a set of five surfaces has been utilized. These horizons are covering the investigated area entirely and are considered to be the bottom boundary of the geological formations. All depths are related to the seismic reference datum.

The surfaces of the *middle and lower Pannonian, Sarmathian* and the *Sandschaller zone* confine the bottom side of sediments that have been deposited in the middle and late Miocene. The basin floor marks the boundary between the sediments of the Neogene and the alpine Carpathian thrust sheets and is therefore a prominent geological boundary and seismic reflector. Figure 8.1 shows the surfaces in a seismic section section, a three dimensional view of the surfaces is given in figure 8.2.

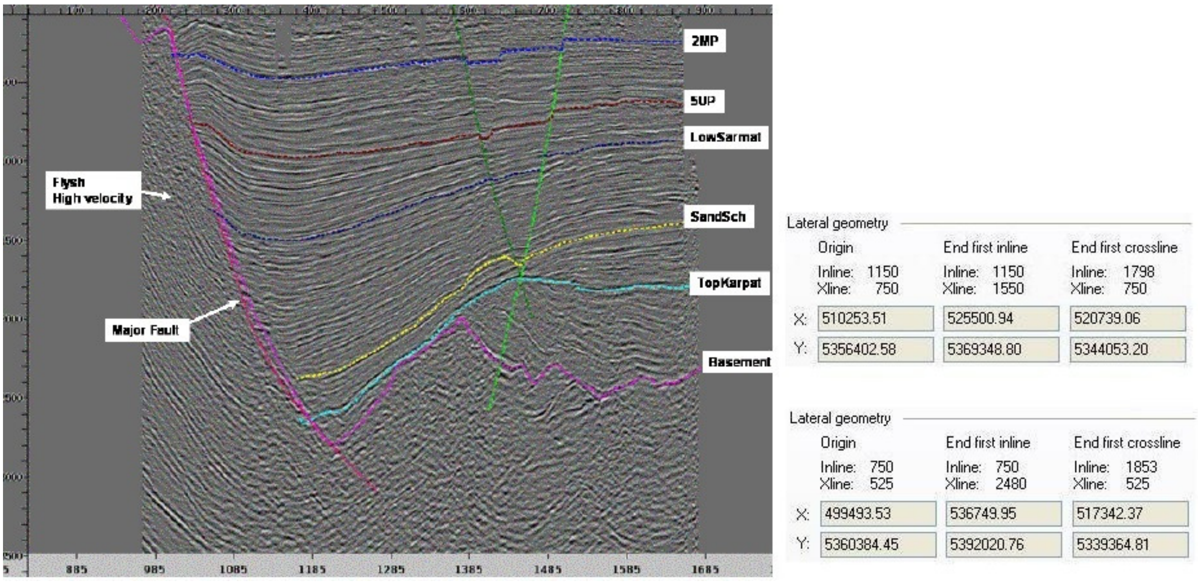

Fig. 8.1, Example of the seismic cross section along crossline 1800. Some prominent horizons, faults and the basement of the sedimentary strata of the Neogene are highlighted. The top Karpathian horizon (light blue) has not been used for model building In the section underneath the basement clearly reflecting horizons can hardly be found. Upper coordinates defines the lateral geometry of the cropped data used in this study, the lower ones are valid for the complete data set.(by courtesy of OMV)

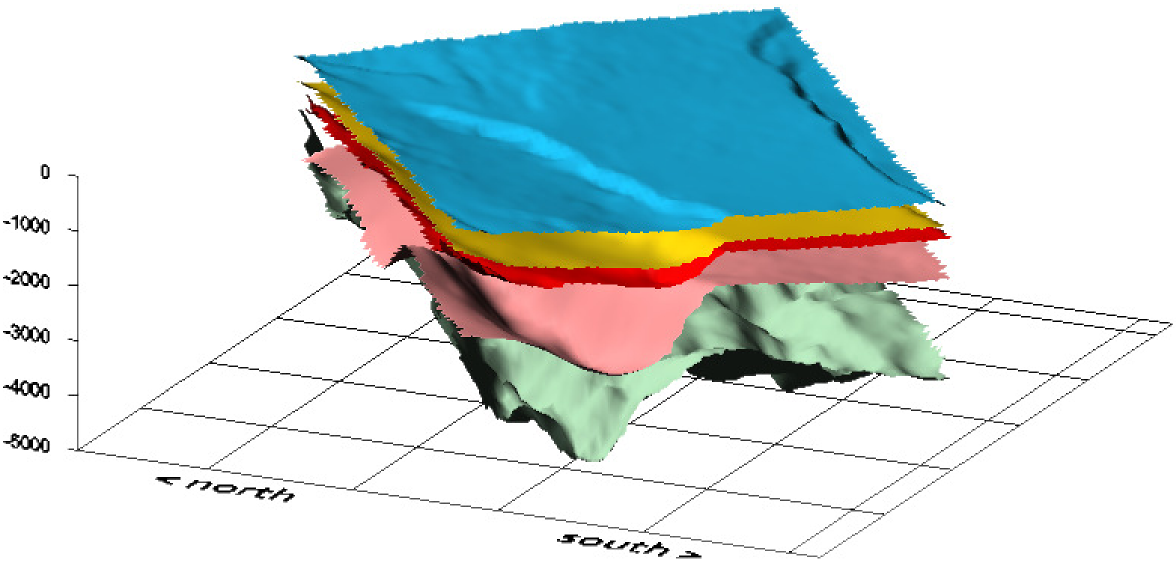

Fig 8.2 3D view of the depth converted surfaces of the Neogene Basin. middle Pannonian (blue), lower Pannonian (yellow), Sarmathian (red), Sandschaller zone (pink) and basement of the Vienna Basin (green). The vertical extension is given in meters, zero is linked to the seismic reference datum set to 130 meters amsl.

8.3 SURFACES OF THE NORTHERN CALCAREOUS ALPS

Due to the lack of precise information on geological units and seismic reflectors in the deep Vienna Basin, the arrangement of major blocks of the structural model has to be estimated. The estimation is governed by three important factors:

1. The first and most important influence for setting up the arrangement of subsurface structures is the general understanding of Vienna Basin within the investigated area. According to Wessely (1993) the Northern Calcareous Alps are arranged in a sequence of folded calcareous units and Gosau layers, see figure 2.3.

2. Available seismic horizons, which define the borders of lithological units entirely or partly

3. Borehole data, that can be assigned to a certain formation and provides velocity information.

Three seismic horizons have been utilized to group the lower part of the model into subunits. These subunits can be assigned to prominent geological formations: the bottom surfaces of *Schönkirchen Tief* and *Goeller thrust sheet* and the top surface of the *Reyersdorfer dolomite*. In addition to the given horizons the necessity of two estimated horizon comes up. The first one represents the *basement of the Northern Calcareous Alps (Base_NCA)* and is used to separate the *Frankenfelser-Lunzer nappe* and *Flysch* from each other. The second estimated horizon, the base of the *Gießhübler monocline (Base_GHM),* establishes the boundary between the *Frankenfelser-Lunzer nappe* and the neighbouring *Gosau layer*. Both horizons have been mapped on a 3D seismic section in an area, where noisy data was dominant and clearly defined reflection could hardly be found. Hence, these horizons are rough estimations that are mainly based on OMV expert knowledge. According to Figure 2.3 the base of the *Gießhübler monocline* is a highly folded, overhanging surface, in particular these folds are assumed to be hydrocarbon reservoirs.

As PETREL 2009 does not allow mapping horizons which are supposed to be overhanging, just one Z-value on a particular set of X-Y-coordinates is possible, vertical or overhanging structures of the *Gießhübler monocline* have been mapped as “near vertical”.

With these five horizons and the Neogene basin floor the following arrangement of geological units according to figure 2.3 can be established (Wessely 1993).

- The *Schönkichen Tief formation* can be considered to be a subunit of the of the *Goeller nappe* and consist of main dolomite. Located right underneath the basin floor it is entirely bounded by given horizons.
- The *Goeller nappe (Tirolikum)* is bordered by the horizons *Schönkirchen Tief* and the Neogene basin floor on its top side and by the horizon *Goeller thrust* sheet on its bottom side and therefore clearly defined. Mainly limestone and dolomite have been found in this formation.
- The *Reyersdorfer dolomite* builds the top of the *Frankenfelser-Lunzer nappe (Bajuvarikum).* The lateral margin is formed by the base of the *Gießhübler monocline* and the *Base_NCA*. The litological build-up is similar to the *Goeller nappe* and consist of main dolomite and limestone.
- The *Giesshübler monocline* is embedded between the Frankenfelser-Lunzer nappe and the Goeller nappe and is therefore clearly defined by the horizons separating it from the neighbouring formations. Being part of the so called Gosau layers the Gießhübler monocline consists of paleozoic sandstones, the seismic velocities in these layers are significantly lower than in the carbonate rock of the adjacent formations.
- Although the *Flysch* encompasses a big part of the model, in a strict sense it is not part of the Calcareous Alps. Within the model it is bordered laterally by the Base_NCA and the Reyersdorfer dolomite, the Neogene Basin floor establishes the top margin.

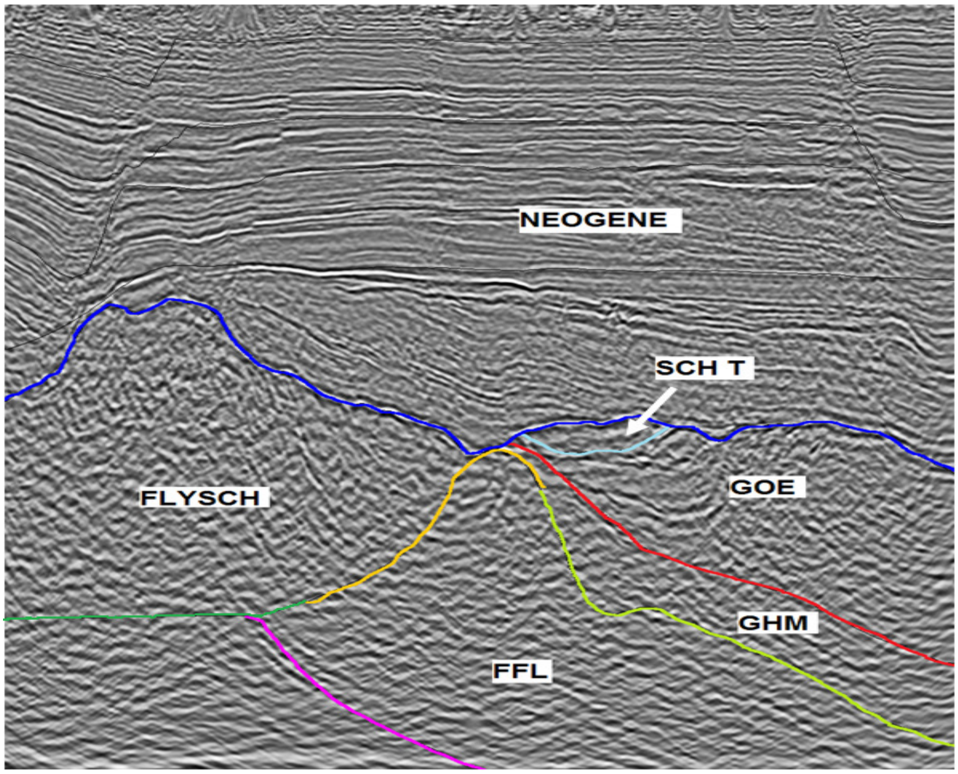

Fig 8.3 Example of a seismic cross section along crossline 800. The area underneath the Neogene Basin floor (dark blue) is subdivided into 5 main blocks. The Schoenkirchen Tief formation (Sch T) and the Goeller nappe (GOR) are entirely defined by given surfaces Schönkirchen Tief (light blue) and Goeller thrust sheet (red). The Frankenfelser-Lunzer nappe (FFL) is bounded by Reyersdorfer dolomite surface (yellow) on its top and by BASE_GHM (light green) and BASE_NCA (dark pink) laterally. Embedded in between the latter and the Goeller nappe lies the Giesshübler monocline (GHM).And finally the flyschzone is bordered by the Reyersdorfer dolomite, the Neogen Basin floor and BASE_NCA. The green thin line is an auxiliary surface, that ensures the intersection of the corresponding surfaces. (Seismic section by courtesy of OMV)

In order to define the five main blocks properly without gaps in between, intersecting surfaces that need to cover the whole area of interest are necessary. Obviously none of the surfaces meets these requirements. Fortunately PETREL 2009 offers the opportunity to create auxiliary surfaces in order to extend surfaces. Moreover intersecting surfaces can be combined using logical commands to create one surface that cover the whole area without any gaps. For exporting the ASCII file format *Earth Vision grid* (extension *.xyz**)** has been used. OMNI 3D demands surface data in ASCII format files containing nothing but 3 columns of X-, Y-, and Z-coordinates. Exporting files in earth vision grid format adds 7 header lines at the top and 2 columns, which contain the indices of the coordinates.
This header lines and columns have to be deleted to make files readable for OMNI 3D. The exported surfaces build the final structural model.

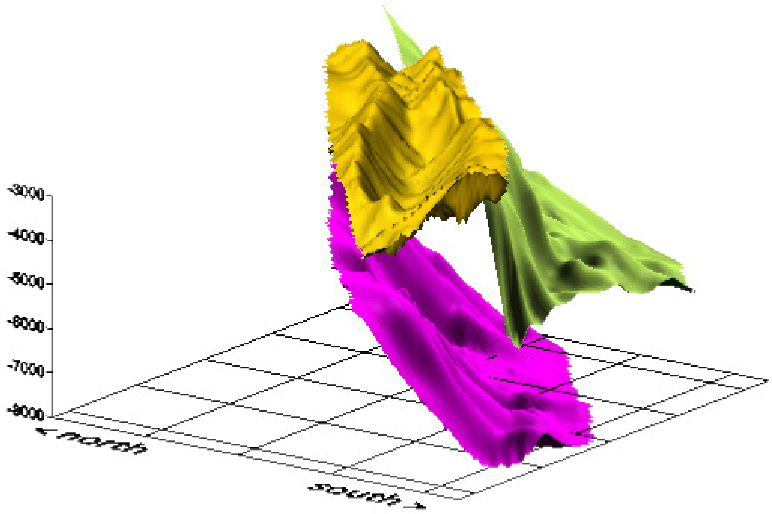

Fig 8.4 3D sketch of the surfaces Reyersdorfer dolomite (yellow), BASE_GHM (green) and BASE_NCA (dark pink), which defines the boundaries of the Frankenfelser-Lunzer nappe. The gaps between the surfaces will be closed by auxiliary surfaces.

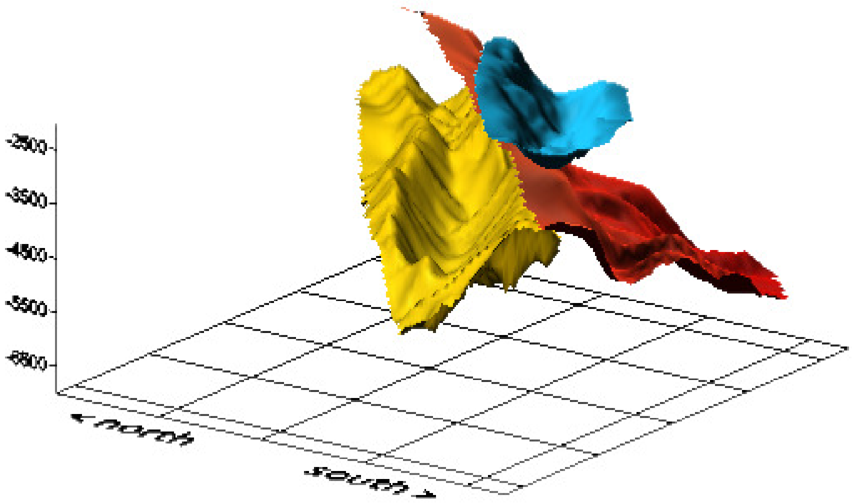

Fig 8.5 3 D sketch of the given horizons of the Northern Calcareous Alps, located directly underneath the Neogene Basin floor: the . Reyersdorfer dolomite (yellow), Goeller thrust sheet (red) and the Schoenkirchen Tief (light blue)

9 VELOCITY MODEL BUILDING

9.1 PREREQUISTES ON THE VELOCITY MODEL

In contrary to surfaces the velocity model has to be in time domain to be readable for OMNI 3D. Nevertheless all available velocity information encompassing checkshot data, sonic log data and the 3D velocity field is given in depth domain. Surfaces have also been converted in depth domain, therefore the whole velocity model is set up in depth domain and will be converted later on. Once having a velocity model either in time or in depth domain, PETREL 2009 provides the opportunity to switch from time to depth and vice versa.

Like the structural model the velocity model will also be subdivided into two parts. Due to dense information and an accurate velocity model of the upper Neogene section, the 3D PSDM interval velocity field gives the upper part reaching from the surface down to the Neogene Basin floor. Velocities assigned to the geological units defined by the lower part of the structural model are obtained by well data analysis. PETREL 2009 allows to fill the space between two surfaces either with an constant velocity value or with linear increasing velocities.

9.2 WELL DATA ANALYSIS

The primary intention of this study was to obtain a velocity model only by checkshot data analysis. The reason was that checkshot surveys have been performed as zero offset surveys, that means the result of the checkshot gives a direct relationship between the depth of the geophone and the wavelet’s travel time over a close to vertical ray path (assuming a vertical well path). Therefore checkshot data is assumed to be very reliable data. But the problem arose that even for wells that are reaching the desired depth, checkshot surveys have not always performed in the deeper parts of the wells. Hence, sonic log gives the opportunity to improve the quality and density of velocity information where checkshot data is leaving gaps.

In addition to these kinds of information also geological well data of tops and bottoms of corresponding formations are provided, which allows to assign depth and velocitiy to a certain lithological unit. In some cases the well has not been drilled through the entire formation of interest, therefore the velocities continuation in areas below the drilling depth is an estimation based on OMV expert knowledge.

Used sonic log data has got resolution more than two orders of magnitude higher than those originating from checkshots. Tthe data sets used in this study have got a vertical sampling interval of 10 cm, whereas checkshots deal with a resolution of 25 meters or are sometimes even irregularly spaced. The dense sampling interval makes sonic log very sensitive on local changes of the adjacent rock. Cracks, cavities or changes in the borehole's cross section could lead to considerable changes of the measured velocity Thus sonic logs produce quite noisy data with a large dynamic range (see figure 9.1). Therefore downsampling and smoothing using a moving average filter was necessary to make both kinds of velocity information comparable and combinable.

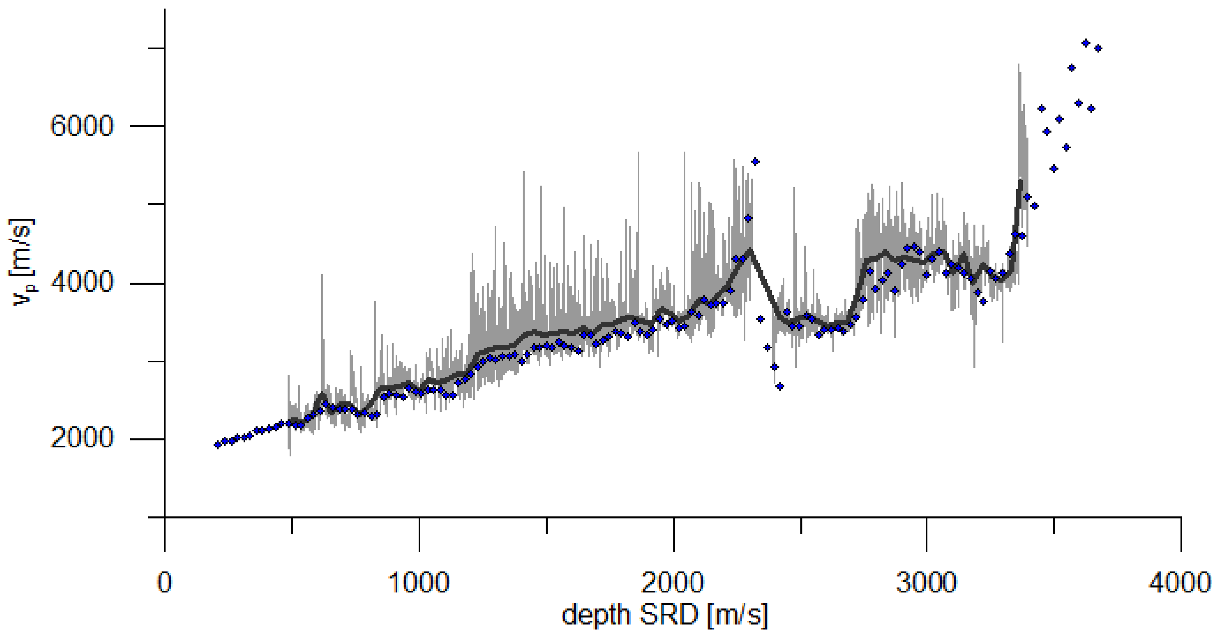

Fig. 9.1, Comparison of p-wave velocities from borehole Ebenthal T001. Noisy raw data with from sonic logging (light grey), downsampled and smoothed sonic log data (dark grey), interval velocities derived from checkshot data (blue dots). The gap of sonic log data at a depth of approximately 2300-2400 meters results from missing data.

9.2.1 FRANKENFELSER-LUNZER NAPPE

In the investigated area the folded structures of Frankenfelser-Lunzer nappe are supposed to be potential hydrocarbon reservoirs and are therefore well explored with several deep reaching boreholes. Checkshot surveys carried out in the wells Strasshof T004, T005 and T006 provide velocity information with a resolution of 25 meters, the corresponding sonic log data was recorded with an vertical sampling interval of 0.1 meters and has been downsampled to the same resolution of the checkshots of 25 meters. The following graphs (figure 9.2a – 9.3c) show the velocity distribution of the corresponding wells derived from checkshots and sonic logs. Also the result of the linear regression is depicted as straight line and defined by the linear equation.

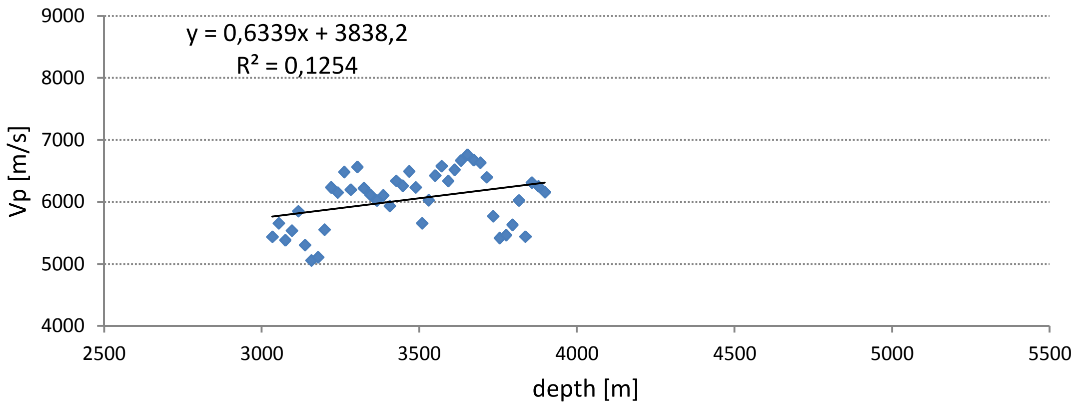

Fig. 9.2a, Strasshof T004 checkshot

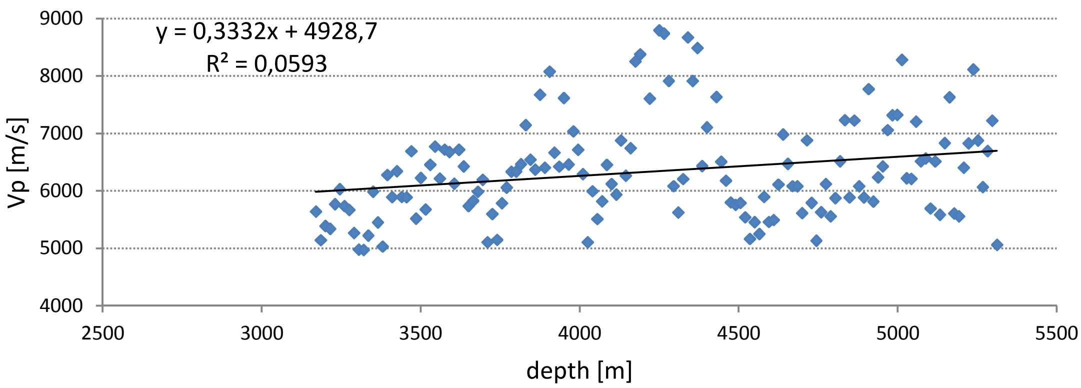

Fig. 9.2b, Strasshof T005 checkshot

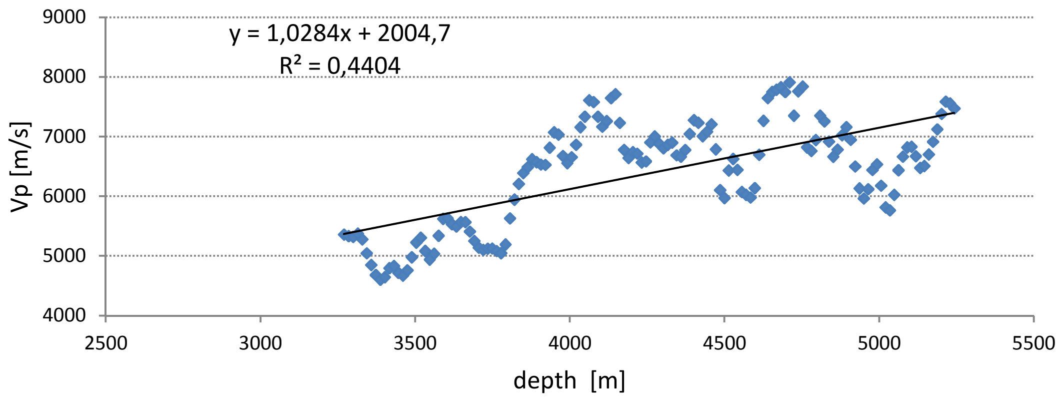

Fig. 9.2c, Strasshof T006 checkshot

Figure 9.2 a-c depicts the distribution of interval velocities derived from checkshot records. The straight line of the linear regression is given by the first grade polynom in each diagramm. The coefficient of determination R^2 helps to evalute the quality of the linear model.

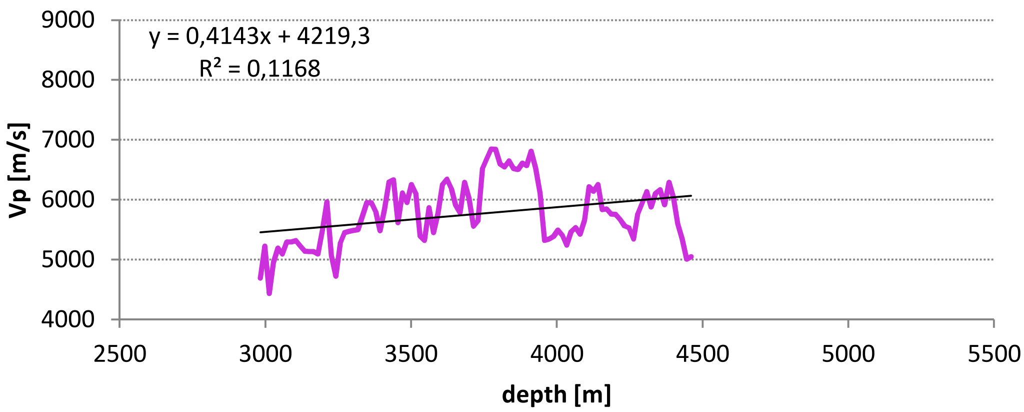

Fig. 9.3a, Strasshof T004 sonic log

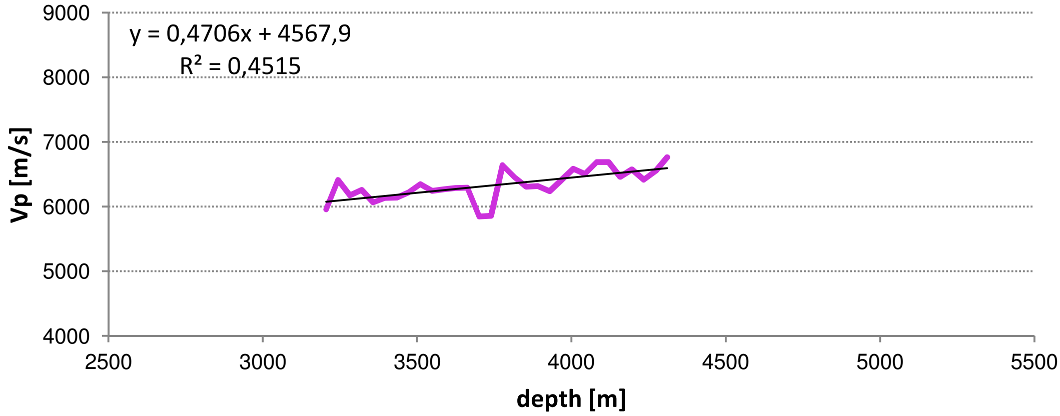

Fig 9.3b, Strasshof T005 sonic log

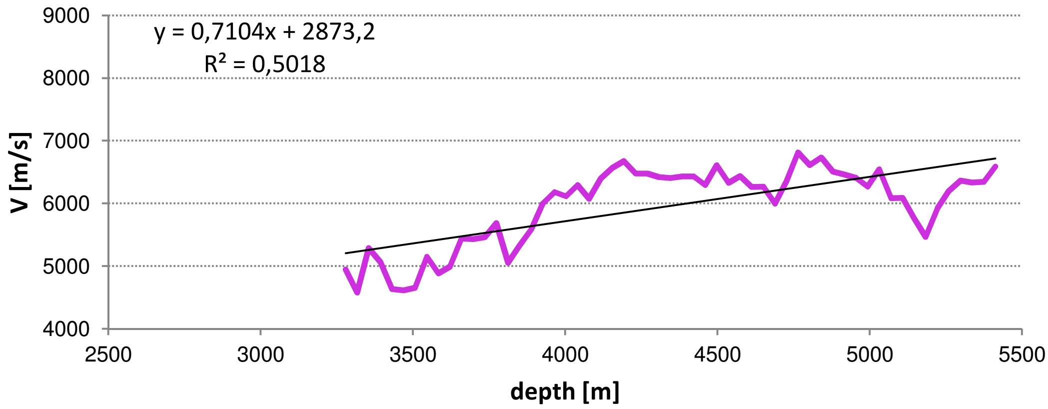

Fig 9.3c Strasshof T006 sonic log

Figure 9.3 a-c shows the interval velocitites derived from from sonic log records. Downsampling to same resolution as checkshot data and smoothing of the raw data eliminated statistical outliers and reduced the dynamical range significantly. The linear modeldetermined by the linear regression equation. The coefficient of determination R^2 is used to evalute the quality of the linear model.

Visual analysis of the diagrams in figures 9.2a-c highlights the big dynamic range of checkshot derived velocities. The fact that the Frankenfelser-Lunzer nappe internally consists of folded and fractured sublayers and nappes could give an explanation for the occurance of velocity changes within rather small distances. The highest velocities of Strasshof T005 (see fig. 9.2b) are reaching values significantly above 8000 meters per second, which is unusually high even for depths deeper than 4000 meters. Those high values can be interpreted as measuring errors that occurred during the acquisition. The significantly lower dynamic range of sonic log data can be explained with the previous filtering procedure. A clear correlation between checkshots and sonic log like the one observed at well Ebenthal T001 (fig 9.1) could not be found in the wells around Strasshof. In order to obtain an equation that fairly represents the velocity increase in greater depths some statistics can give support.

In actual rock the velocity increases with increasing depth as a consequence of compaction. Thus the velocity gradient is a highly variable parameter. The internal buildup of the Frankenfelser-Lunzer nappe is very heterogeneous, which is also evident in the velocity values along the analyzed well paths (see fig 9.2a-c, 9.3a-c), thus an exact mathematical description of the velocity increase can hardly be found. Compaction as a consequence of load of overlying rock cannot occur infinitely, therefore a linear regression of measured values poorly describes the actual velocity distribution.

Nevertheless PETREL2009 allows velocity definition within a model just as constant value or linear increasing velocity. Hence the linear regression of the velocity values of each well is calculated and given as a first grade polynomial (see within fig 9.2, 9.3).

well name	formation top SRD [m]	v_P sonic log [m/s]		v_P check shots [m/s]	
		measured	calulated	measured	calculated
Strasshof T004	2980	4692	5453	5440	5727
Strasshof T005	3205	5954	6075	5641	5995
Strasshof T006	3279	4942	5202	5359	5376

Tab 9.1a Seismic velocities on the top of the Frankenfelser-Lunzer nappe.

well name	depth SRD [m]	v_P sonic log [m/s]		v_P check shots [m/s]	
		measured	calulated	measured	calculated
Strasshof T004	3800	6594	5793	5653	6247
Strasshof T005	3800	6456	6356	6339	5956
Strasshof T006	3800	5053	5572	5631	5911

Tab 9.1b Seismic velocties within the Frankenfelser-Lunzer nappe at a depth of 3800 meters

Comparing the velocity values actually acquired with velocities calculated according to the equations given by the linear regressions still leaves significant uncertainties on which polynomial represent best real velocity increase. Differences are covering a range of more than +/- 500ms^{-1}. Checkshot derived data from well Strasshof T005 gives the lowest residuals between measured and calculated value of approximately 100 ms^{-1}, but considering the dyamic range reaching from 4000 ms^{-1} to 9000 ms^{-1} this can be interpreted as random hit.

The quality of the linear regression can also be evaluted with the help of the *coefficient of determination* R^2 which describes the fraction of the complete data series, that can be explained with the model. With an R^2 of 0.059 less than 6 percent of the checkshot data of Strasshof T005 can be explained with the derived linear model, whereas sonic log data of Strasshof T006 (R^2 = 0.5018) gives the best approximation.

Considering these uncertainties the final decision was to calculate the mean values of the six polynomials and use it for the entire formation.

	Strasshof T004	Strasshof T005	Strasshof T006	mean
check shot	v = 0,634z+3838	v = 0,332z + 4928	v = 1,028z +2004	**v=0,444z + 3738**
sonic log	v= 0,414z + 4219	v = 0,471z +4567	v = 0,71z +2873,2	

Tab 9.2 List of polynomials derived from velocity data analyisis. The finally used polynomial has been obtained calculating the mean value from all wells. The z value is given in meters.

9.2.2 GOELLER NAPPE

In contrary to the Frankenfelser-Lunzer nappe the Goeller nappe gives poor information for this thesis' purposes. Several borholes have been drilled to a depth to reach this formation, but in most cases sonic logging or checkshot surveys have not been performed or stopped before the Neogene basin floor has been crossed in a way that reliable data can be provided.

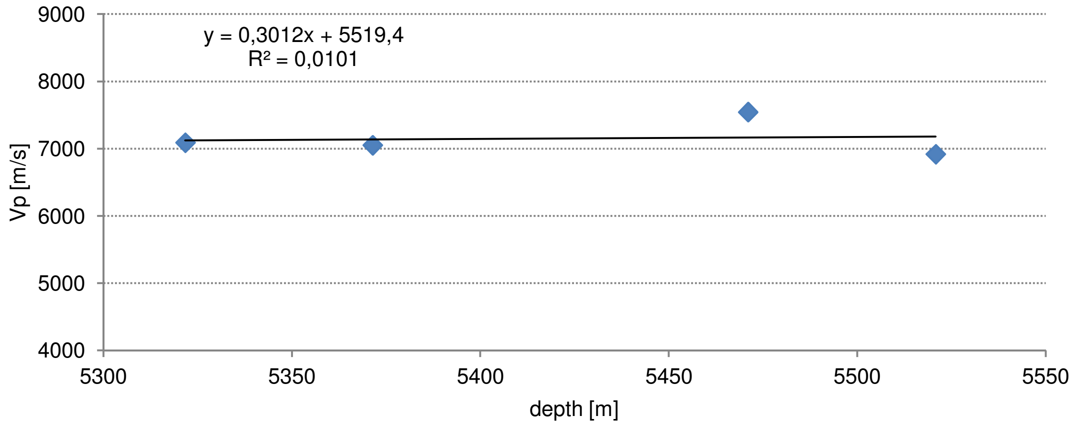

Fig. 9.4, Checkshot derived values and linear regression of well Gänserndorf ÜT003a. The low coefficient of determination of one percent can be explained with the low number of data points.

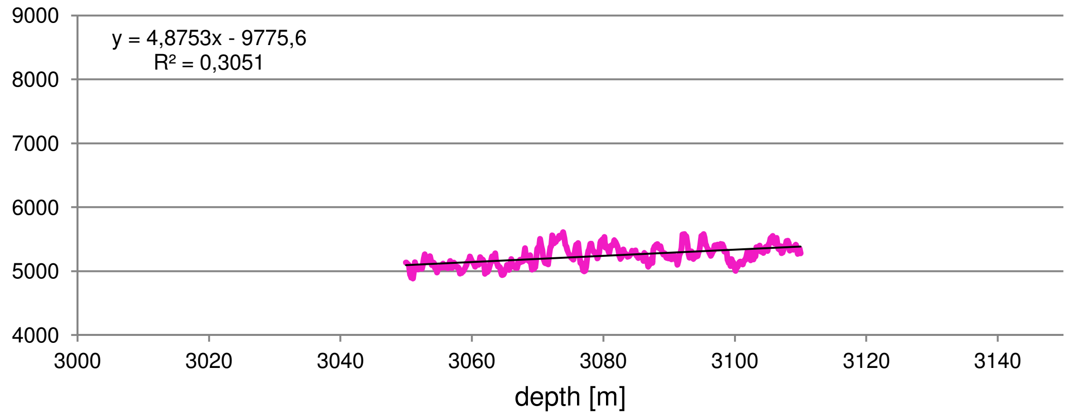

Fig. 9.5, Sonic log derived velocity values and linear regression of well Strasshof T002. Data has not been downsampled because of the small amount of data points and the narrow vertical extension covered by them. Note the different scaling of the x-Axis of figure 9.4 and 9.5.

Since the borehole Gänserndorf ÜT003a is the only well that provides checkshot derived velocities, it has been used for data analysis although the amount of data points is very low. It is located outside of the investigated area, but still it reaches the Goeller nappe at a depth of approximately 5200 meters after crossing the Glinzendorfer syncline and provides velocity information of the uppermost 200 meters of the formation.The slope of the linear regression is lower compared to those obtained in Frankenfelser-Lunzer nappe (fig 9.4). This becomes more clear if one considers that in actual rock the curve of velocity increase is not a linear function but flattens with increasing depth.

Sonic log data depicted in figure 9.5 just covers the uppermost 60 meters of the Goeller nappe underneath the basin floor. Hence no velocity increase can be obtained within this small distance, but it gives punctual information of mean velocity values on top of the geological unit.

Within the investigated area the top layer of the Goeller nappe is located directely underneath the Neogene basin floor at a depth of approximately 3000 meters. Assumig a linear velocity increase, the velocity at the top of the formation can be calculated according to the linear regression. The obtained value would be approximately 6400 ms^{-1} which is not evident in sonic log data having a mean value of 5240 ms^{-1}. Therefore the polynomial of the checkshot data can not be considered to be representative for the velocity increase of the Goeller nappe.

Under the assumption of a lithological buildup and vertical extension similar to the Frankenfelser-Lunzer nappe the decision to choose the same polynomial in order to describe the velocity distribution of the Goeller nappe seems to be arguable.

9.2.3 SCHOENKIRCHEN TIEF

The Schönkirchen Tief formation, being part of the Goeller nappe, is well known as an oil and gas reservoir. Sonic logs come from borehole Schoenkirchen T001 but there has no checkshot data been provided for this geological unit.

Sonic log data in this formation covers also just the uppermost 60 meters and is therefore not representative for the velocity increase. The entire formation consits of main dolomite where no significant rise of velocity is expected. Hence the Schönkirchen Tief is assumed to be an area of one constant velocity value defined by the mean value of the sonic log. In the final model the velocity of the Schönkirchen Tief formation is set to 6070 ms^{-1}.

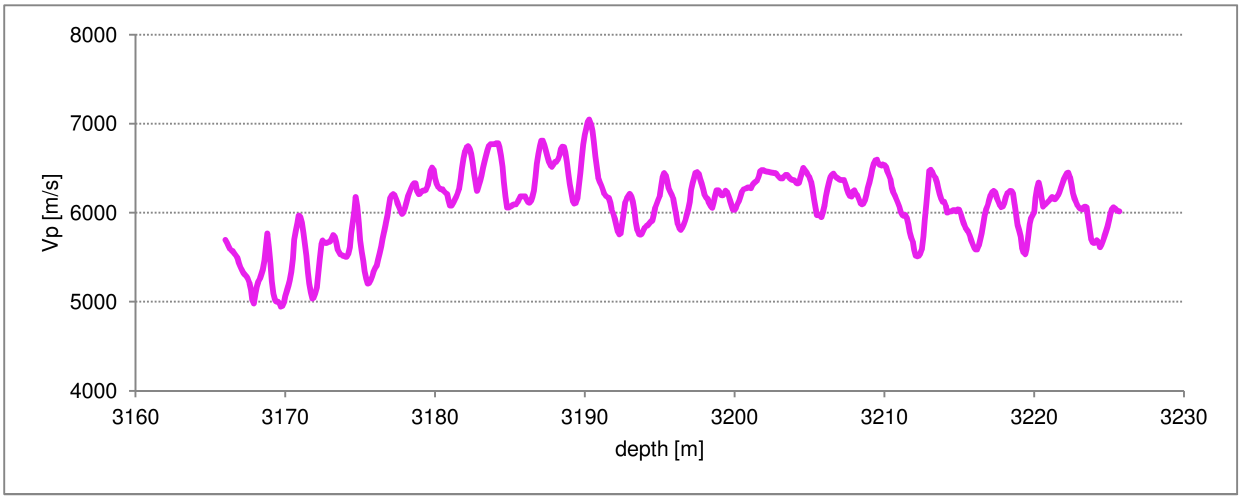

Fig. 9.6, Sonic log record of borehole Schönkirchen T001. Because of the small vertical distance covered by the sonic log the mean value is assigned to the entire formation.

9.2.4 FLYSCH AND GIESSHÜBLER MONOCLINE

Although some deep reaching boreholes are hitting the Flysch zone located in the north-west of the area of interest, none of them provides reliable data. Punctually measured sonic log data in shallow depth underneath the formation's top surface at a depth of 4320 meters gives a seismic veloctiy of approximately 4400 ms^{-1}. But the Flysch zone is considered to be a section of rather high seismic velocities, therefore th obtained velocity is supposed to be too low. Based on OMV expert knowledge the velocity is set to 5500 ms^{-1} and increases up to 6700 ms^{-1} till a depth of approximately 6200 meters, which is equivalent to a time level of 4000 milliseconds. The corresponding polynomial is given with: $v_P = 0{,}638z + 2742$

Due to the lack of velocity information and too low drilling depth of the corresponding wells no reliable data on the Giesshübler monocline is available. Sonic log of well Strasshof T002 indicates a velocity of approximately 4100 ms^{-1} at the top of the formation in a depth of 3100 meters. The Giesshübler monocline consists of paleozoic seditments with significantly lower seismic velocities than the adjacent Frankenfelser-Lunzer nappe. A velocity increase to a maximum of 5700 meters at the bottom of the monocline at 6100 meters depth is assumed. The corresponding polynomial is: $v_P = 0{,}5z + 2550$

9.3 SETTING UP THE VELOCITY MODEL

As compaction as a consequence of load of the overlying rock cannot occurr infinitely, the velocity increase within the model has to stop in a certain depth and turns into a constant value. Due to the fact that none of the used wells are reaching the depth where velocty increase diminishes clearly, the decision was to use constant values below a time level of 4000 milliseconds, the corresponding depth is approximately 6200 meters. The velocity model itself covers a vertical distance in time of 5000 milliseconds, the vertical extension in depth domain is approximately 7500 meters.

NEOGENE	3D PSDM VELOCITY FIELD
FRANKENFELSER-LUNZER NAPPE	V_P=0,444z + 3738
FRANKENFELSER-LUNZER NAPPE 4000 ms	6490 ms^{-1}
GOELLER NAPPE	V_P=0,444z + 3738
SCHOENKIRCHEN TIEF	6070 ms^{-1}
FLYSCH	V_P = 0,63z + 2742
FLYSCH 4000 ms	6730ms^{-1}
GIESSHUEBLER MONOCLINE	V_P = 0,5z + 2550

Tab 9.3, List of input parameters of the corresponding structures for setting up the velocity model with PETREL 2009

With the the parameters given in table 9.3, the PSDM interval velocity field and the surfaces of the structural model PETREL 2009 is able to run the velocity model. The lateral resolution is set from 50 meters to 200 meters, the vertical resolution gets decreased from 5 meters to 50 meters. This helps to keep the filesize low and still ensures a fairly accurate model. The velocity is created in depth domain, but it has been stored in time domain to fullfill the demands of OMNI 3D.

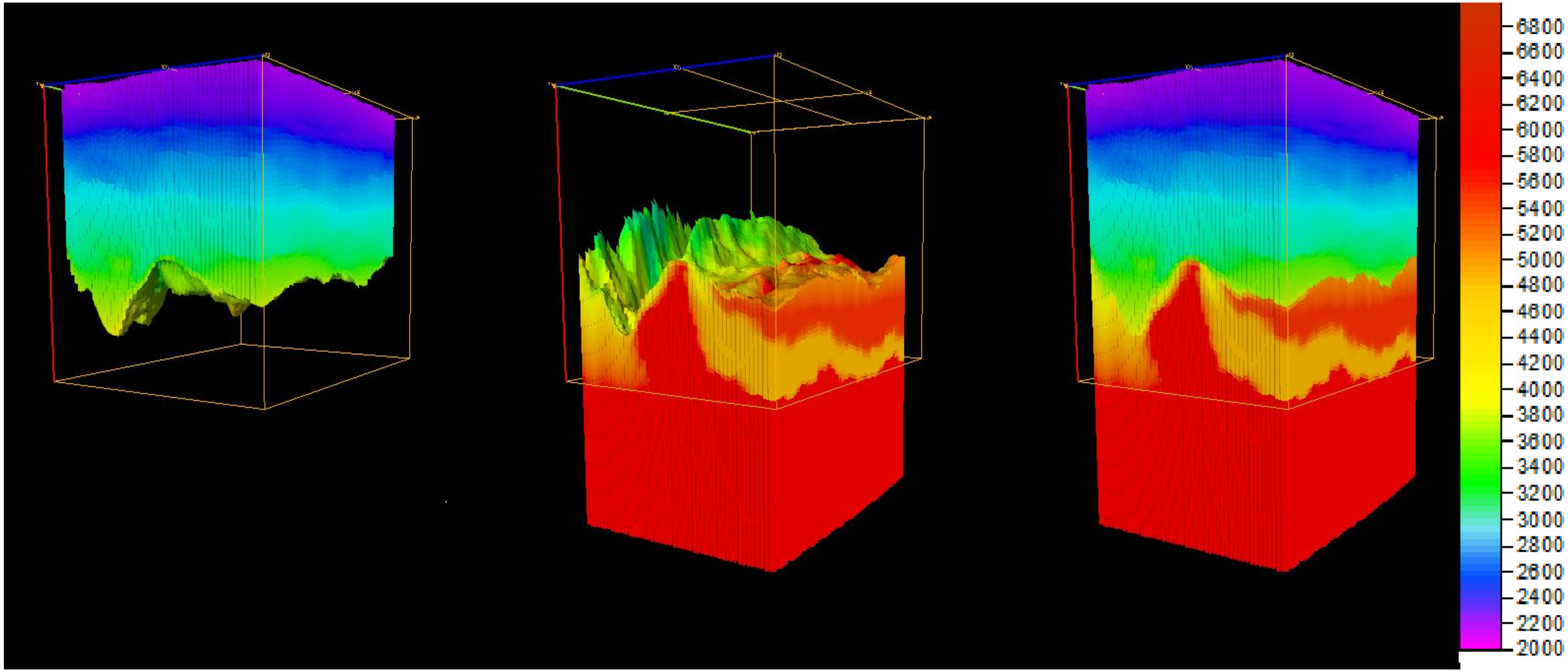

Fig 9.7, Final interval velocity model in time domain. The upper is given by 3D PSDM velocity field (left) reaching from the surface to the Neogene basin floor. The lower part (middle) is defined by the results of well data analysis. Linking the two parts together yields the final velocity model (right).Velocity values are covering a range fromm 2000ms^{-1} up to approximately 7000ms^{-1}

The obtained velocity field has been exported in Petrel ASCII format *GsdLib:*

header row			
X	*Y*	*Z*	*velocity value*
...	...	...	...

OMNI 3D requires velocity data in a ASCII format defined as followed:

LOC X1, Y1		
velocity value	*Z*	*Q*
…	…	...
…	…	…
LOC X1, Y2		
…	…	…

The conversion into OMNI 3D format has been performed with a MatLab script. The final file has to have the extension **.vin* for an interval velocity file or the extension **.vag* for an average velocity file. The Q-values are set to 50 by default.

10 APPLICATION OF THE ATTENUATION MODEL

The fact that the amplitude of seismic waves with shorter wavelengths ist getting stronger attenuated than those with longer wavelengths leads to the undesired effect that seismic sections of deeper areas are suffering on low spatial resolution as a consequence of lack of high frequencies. In order to address this problem an attenuation model of the investigated area should help to quantify the decay of a wavelet's amplitude. Seismic records coming from vertical seismic profiling surveys (VSP) of two deep reaching boreholes have been analyzed to achieve the quality factor Q in various depths. The fact that VSP survey is recording a seismic wave in regularly spaced distances along a vertical well path makes VSP data suitable for attenuation analysis. All calculations for Q factor determination have been carried out with MatLab.

10.1 SPECTRAL RATIO METHOD

In this method the *amplitude spectrum A(Z,f)* of a seismic trace on certain geophone *depth level Z* is calculated using a FFT algorithm. The exponential decay of the amplitude spectrum *A(Z,f)* compared to a reference amplitude spectrum $A_0(Z_0,f)$ at a shallower geophone depth level Z_0 is given with

$$A(Z,f) = A_0(Z_0,f)e^{-\alpha(Z-Z_0)} \qquad \text{(Eq. 10.1)}$$

Following Eq. 6.6 we can rewrite this to

$$\ln\frac{A(Z,f)}{A(Z_0,f)} = \frac{-\pi f(T-T_0)}{Q} \qquad \text{(Eq. 10.2)}$$

Assuming a strict exponential decay the logarithmic ratio of A(Z,f) and $A_0(Z_0,f)$ crossplotted versus the *frequency f* gives a straight line. The *slope k* of the straight line is calculated by a least square fit from the data points in the crossplot (Schön 1996, 283ff)

$$\ln\frac{A(Z,f)}{A(Z_0,f)} = k\,.\,f + d \qquad \text{(Eq. 10.3)}$$

Hence the quality factor Q can be calculated as follows

$$Q = \frac{-\pi(T - T_0)}{k} \qquad \text{(Eq. 10.4)}$$

In case of an ideal elastic medium the ratios between the wavelets amplitude recorded in two different depths are constant over the whole frequency range and the slope k is approaching zero. Hence a high quality factor Q indicates an elastic medium with low attenuation. According to Schön (1996) Q values for between 30 and 100 for porous sedimentary rock and 100 to 250 for compacted sedimentary rock are a realistic assumption.

Following De et al (1994) the spectral ratio method applied to VSP data has some demands on data quality and acquisition parameter.

1) Constant source waveform for every recorded trace
2) Constant coupling between geophone and the adjacent rock
3) No interference from reflected waves and multiples
4) The quality factor Q is independent on frequency, meaning that Eq 10.3 is a linear function with a constant value for k
5) Negligible noise level, which means that the signal has to be significantly higher than random noise
6) No variation in stratigraphic filtering within the investigated area

This method is encountering for amplitude decay with exponential characteristics with respect to the frequency. Attenuating effects that are independent on frequency are causing a certain offset on the straight line, but have no influence on the slope. Hence, under the assumption that spherical spreading is independent on frequency it is getting automatically eliminated, if the spectral ratio method is applied. Furthermore the assumption has been taken, that the path of the seismic wave is close to vertical and that energy loss as a consequence of refraction is negligible (De et al 1994).

The boundary between the Neogene and Northern Calcareous Alps (NCA) represents the most prominent discontinuity of acoustic impedance within the model at a depth of approximately 3000 meters. Hence, the expected energy loss as a consequence of reflection has to be estimated and the transmission coefficient has to be calculated.

Following Schön (1996) the density of solid dolomite (NCA) is given with 2,8 – 2,85 g/cm^3 and for sediment rock like the Neogene Basin fill in a depth of approximately 3000 meters is 2,6 – 2,8 g/cm^3. The density of compactable sediment rock can also be determined be estimating the porosity $\emptyset_z$ using Eq. 10.5

$$\emptyset_z = \emptyset_0 . \exp\,(B_1 . z) \qquad \text{Eq. 10.5}$$

where z is the burial depth, $\emptyset_0$ is the initial porosity at the surface and B_1 is an empirical factor describing the compactibility of the sediments.

B_1 is a highly variable material parameter depending on rock material, grain size and shape. An example given in Schön (1996, 24) sets the initial porosity of sediments to 49 %, the empirical factor B_1 is given with 0,45. In depth of 3000 meters this would yield a remaining density of 12.7 percent. Assuming a average matrix density ρ_{matrix} of 2,8 g/cm^3 and pores saturated with water (ρ_w=1) and applying Eq 10.6 gives an density ρ of 2,57 g/cm^3, for the sediments of the Neogene at the Basin floor, which is slightly lower than the values suggested above.

$$\rho = \rho_{\mathrm{matrix}}(1 - \emptyset_z) + \rho_{\mathrm{w}} . \emptyset_z \qquad \text{Eq. 10.6}$$

An average density of 2,66 g/cm^3 for the Neogene sediments and 2,84 g/cm^3 for the dolomite Northern Calcareous seem to be arguable. Seismic velocities have been taken from the velocity model defined in chapter 9. Applying Eq. 6.2 gives the transmission coefficient T and reflection coefficient R:

ρ NCA	ρ NCA	v Neogene [m/s]	v NCA[m/s]	T	R
2,66 g/cm³	2,84 g/cm³	4400 m/s	5050 m /s	0,9	0,1

Tab 10.1.: Estimation of transmission and reflection coefficient at the Neogene Basin floor

Due to the fact that the reflection coefficient does not exceed 10 percent, the amount of energy lost at the interfaces between the Neogene Basin fill and the dolomitic structures of the Northern Calcareous Alps seems to be negligible for Q factor determination. Thus amplitude loss as a consequence of reflection will not be considered in the following Q value analysis (Schön 1996).

10.2 DATA ANALYSIS

In order to obtain a set of Q values assigned to a certain depth the VSP data of wells Strasshof Tief 006 and Strasshof Tief 004 have been used. Both boreholes a reaching a depth significantly lower than the Neogen Basin floor and provide VSP data with high signal-to-noise ratio. Table 10.1 gives the main well parameters.

well	Strasshof Tief 004	Strasshof Tief 006
SRD	130 m amsl	130 m amsl
elevation log zero	160 m amsl	163,4 m amsl
total number of traces	168	332
receiver spacing	25 m	15 m
natural receiver frequency	20 Hz	20Hz
max. recording time	5000 ms	5000 ms
sampling interval	1 ms	1 ms
depth first trace SRD	30 m	516,6 m
total well depth	4516 m	5146 m

Tab. 10.1, Borehole and VSP parameter of wells Strassof T004 and T006

The data analysis performed follows five steps:

1. Firstbreak picking and time shifting
2. Stacking and tapering
3. Computing of amplitude spectra and logarithmic ratios
4. Determination of frequency range of linear increase and slope calculation
5. Calculating Q values

The following figures originate from VSP data from borehole Strasshof T004

<u>Firstbreak picking and timeshifting</u>

Picking the time of the first arrival of the wavelet has been done with PETREL 2009, the firstbreaks are stored in an ASCII file in two columns containing the trace number and time of zero-crossing. There are three reasons for picking the firstbreaks. The first reason is that scattered traces or traces with high signal-to-noise ratio would significantly degrade the quality of Q determination, hence the firstbreaks of these traces have not been picked (fig 10.1). Only trace numbers having their firstbreak time stored will be further on used for the calculation. Secondly, in order to enhance the signal-to-noise a set of 10 traces are stacked to one single trace. To ensure that the signal of every trace got the same duration, the firstbreaks are shifted to the same time (fig 10.2). The third reason is, that according to Eq. 10.4 the difference in time between firstbreaks is essential for Q factor calculation.

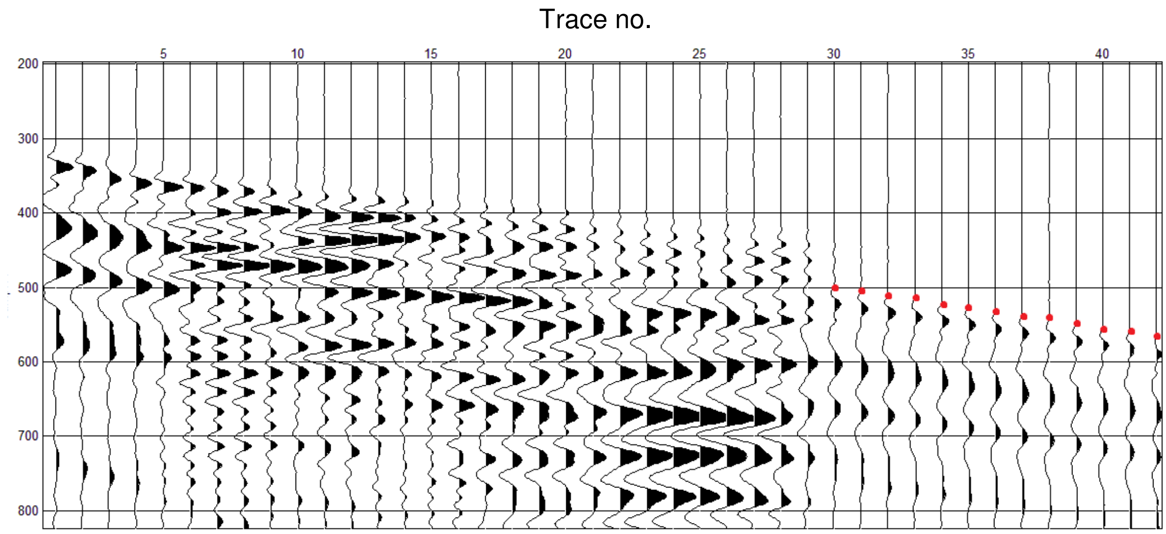

Fig 10.1, First arrivals. The scattered traces no. 1 to 29 result from reverberation from the iron casing and will be not present after time delay correction. Valid traces are marked with firstbreak picks (red) and start at trace no. 30.

Trace no.

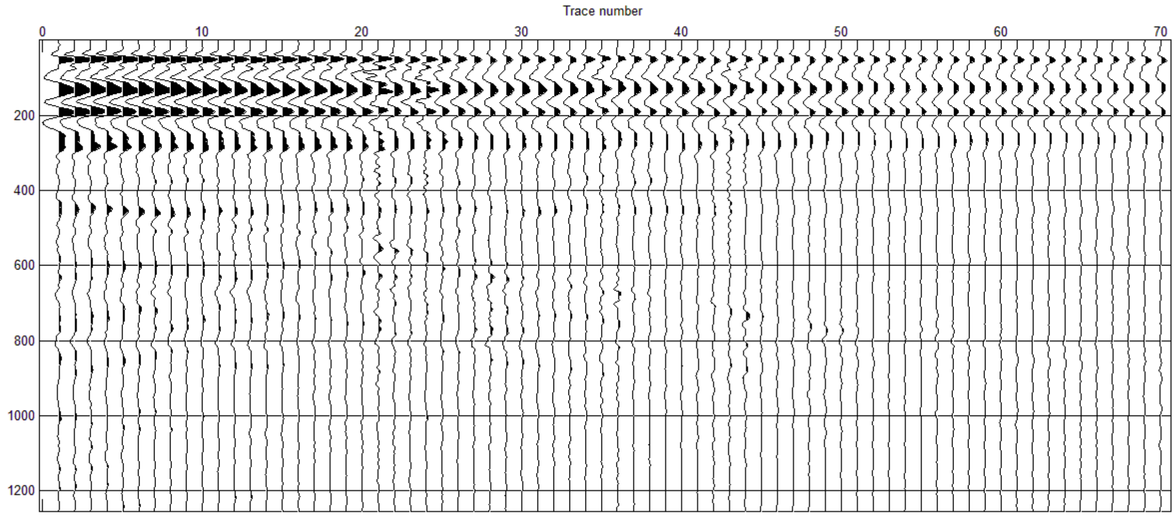

Fig 10.2, First arrivals after timeshifting. Scattered traces 1-29 have been deleted, trace No. 1 is equal th trace no. 30 in fig 10.1. The maximum deflections have been shifted to the same position. The traces are prepared for stacking.

<u>Stacking and tapering</u>

The vertical distance between two traces is 25 meters for well Strasshof T004 respectively 15 meters for well Strasshof T006. In both cases the vertical distance is too small to detect a reliable loss of amplitude as a consequence of absorption. Therefore ten traces are getting stacked to one single trace. The mean value of the corresponding first arrival times are assigned to the newly stacked trace. The vertical distance between two traces now is 250 respectively 150 meters, which should allow a detectable decay of the amplitude caused by absorption. Furthermore stacking improves the signal-to-noise significantly. The data set of Strasshof T004 consits of 15 stacked traces and Strasshof T006 encompasses 28 stacked traces. The duration of one trace of the VSP section is approximately 5000 ms, the information needed for Q determination with the spectral ratio method is supposed to be in the first arrivals of the seismic wave within the first 150 milliseconds. The information recorded later contains mainly residuals from reflections and multiples which reduces the data quality. In order to find the best results the traces have been set to zero after a duration of 65 ms respectively 70 ms, 150 ms and 950 ms. Finally, a linear taper function has been applied to the first and to the last ten samples of every trace to suppress aliasing effects occurring during the Fast Fourier Transformation (FFT) (fig 10.3).

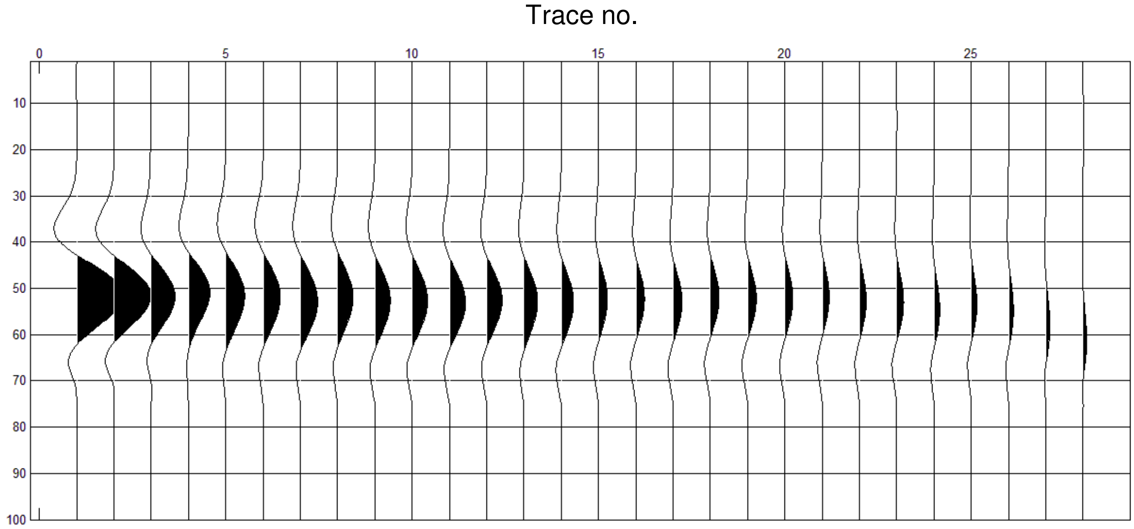

Fig 10.3, After a taper function with a window size of 70 ms only the first periodic cycle remains on the trace, all other values are set to zero. A linear taper is applied to the following 10 samples in order to avoid the arising of aliasing effects during FFT.

Computing amplitude spectra and logarithmic ratios

The amplitude spectra of the stacked traced are calculated using the FFT function in MatLab. The FFT function produces complex values, for the amplitude spectra the absolute value has to be calculated. The sampling interval during the data acquisition was set to 1 ms, following the Nyquist theorem the upper limit of the frequency range is 500 Hz, which is sufficiently high enough. Frequencies higher than 100 Hz are not expected to have significant amplitudes, the natural frequency of the receivers is given with 20 Hz.

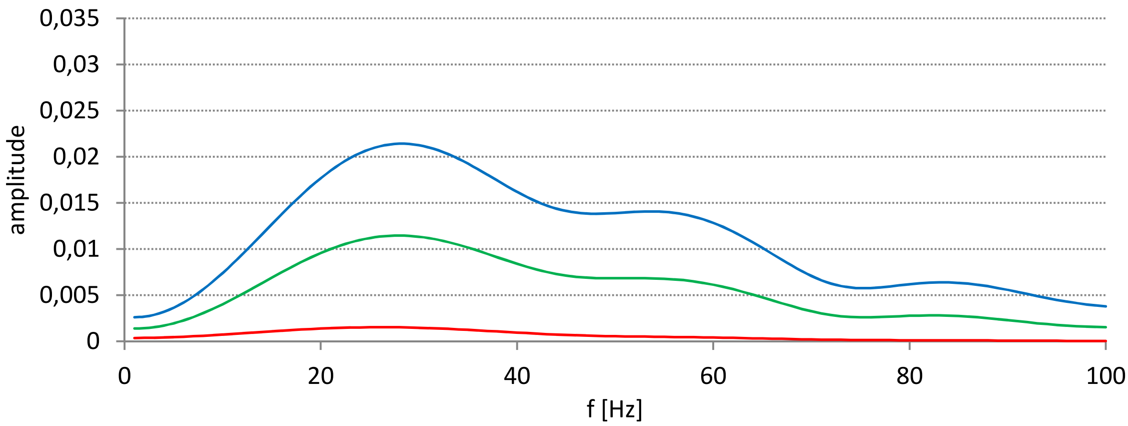

Fig 10.4a, Length of taper window function: 70 ms

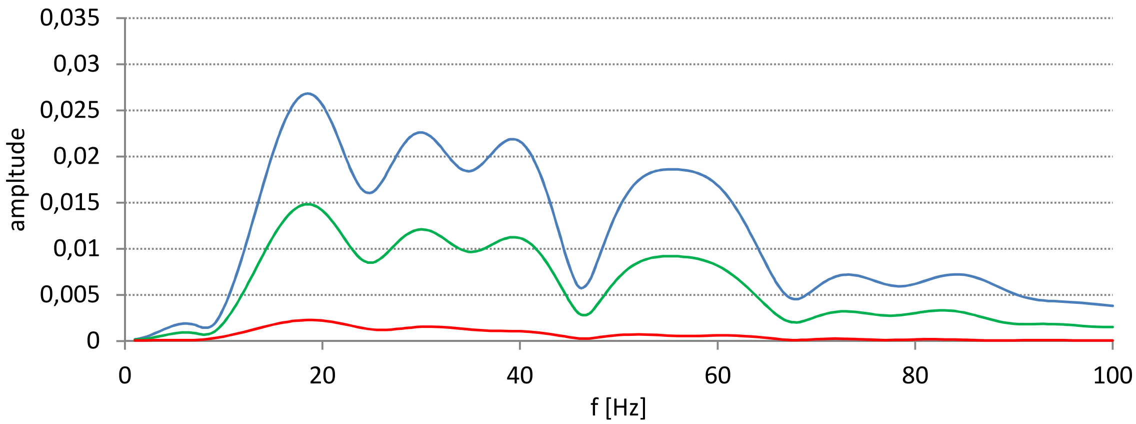

Fig 10.4b, Length of taper window function: 150 ms

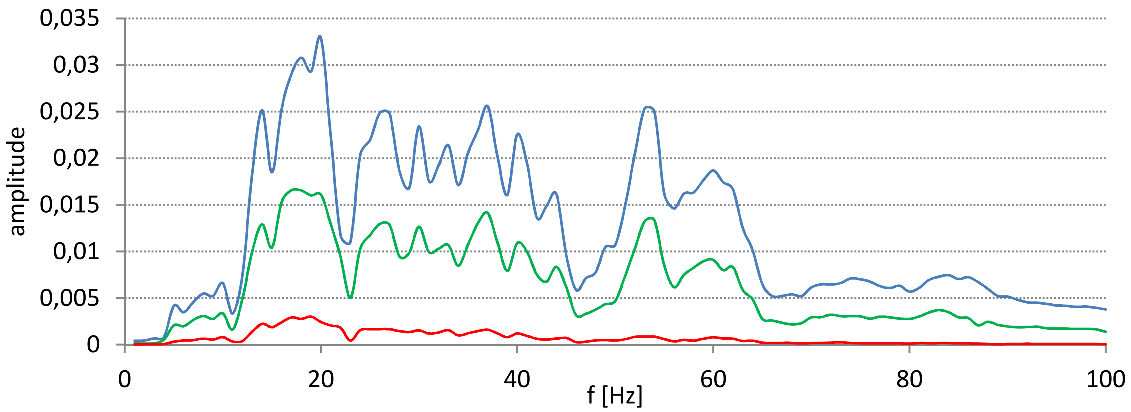

Fig 10.4c, Length of taper window function: 950 ms, entire trace.

Fig 10.4a-c, The diagrams show examples of amplitude spectra of the same stacked traces of well Strasshof T004, but with different taper length. The total signal length is set to 1000 ms, values lying out of the taper window are set to zero. The blue spectra are assigned to a depth of 380 meters, the green originate from a 629 meters and red spectra come from a depth of 1880 meters. For the sake of clarity not all calculated spectra are depicted.

In fig 10.4a the smooth spectra of the first 70ms of the traces are depicted, which encompass one full periodic cycle. The more noisy spectra of the entire trace is shown in fig.10.4d. Multiple reflections and residuals of the upcoming wavefield could give an explanation for the scattered spectra.

Calculating the logarithmic ratio between two amplitude spectra should give a linear decreasing line, the frequency range of linearity should cover the frequency range with the highest amplitude. Two kinds of ratios have been achieved from the amplitude spectra which are now defined as follows:

- ***ratios type A*** ***ln (A_n/A_1)***
- ***ratios type B*** ***ln (A_{n+1}/A_n)***

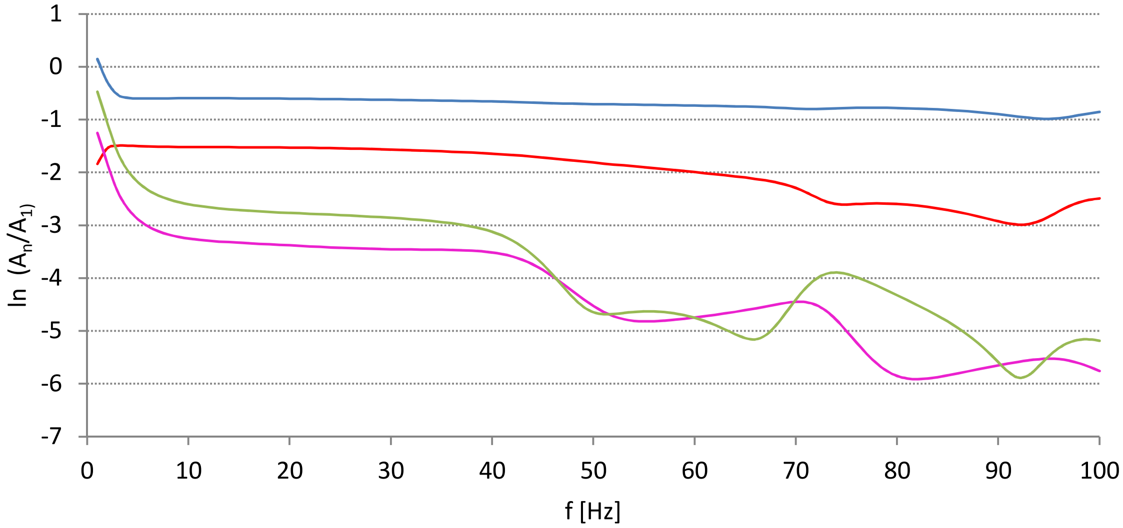

Fig. 10.5a, Examples of logarithmic ratios between the A_n and A_1(type A). Corresponding depths are blue:380m-679m, red: 380m-1129m, green: 380m-2129m, pink: 380m-3379m

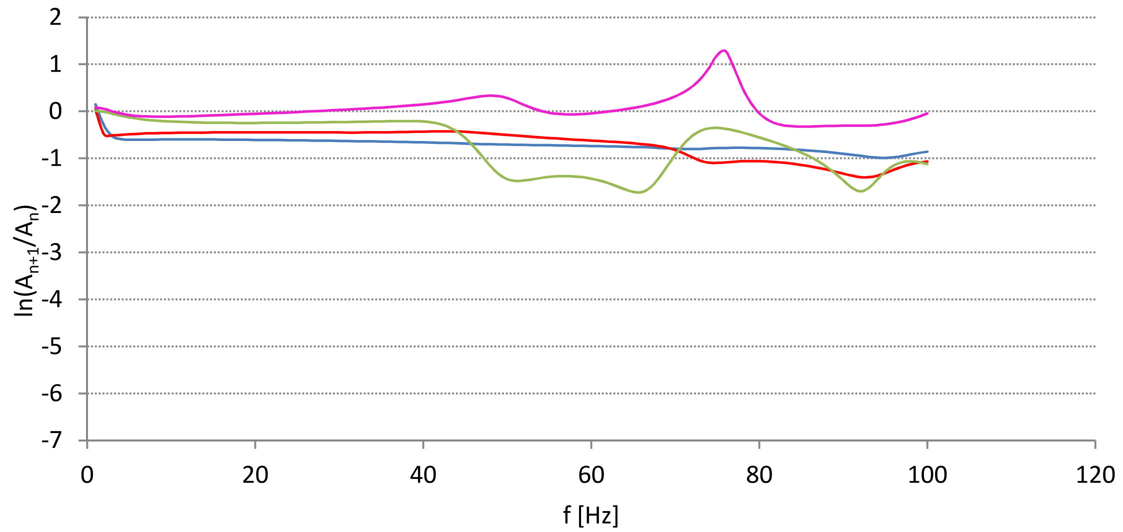

FiFig. 10.5b, Examples of logarithmic ratios between the A_{n+1} and A_n (type B). Corresponding depth are blue: 380m-679m, red: 879m-1129m, green: 1879m-2129m, pink: 3129m-3379m

Determination of frequency range of linear increase and slope calculation

In fig. 10.5a-b some examples of logarithmic ratios are shown derived from spectra originating from traces with 70 ms length. For a clearer illustration not all 14 ratios are depicted. In the line with theory one can find a frequency range between 10 Hz and 40 Hz that is fairly linear. This covers perfectly the range of the highest amplitude which is approximately at 25 Hz and the natural frequency of the used receivers, which is given with 20 Hz. The MatLab script *linreg.m* computes a linear regression over the defined frequency range and produces a set of values that corresponds to the slopes of each logarithmic ratio.

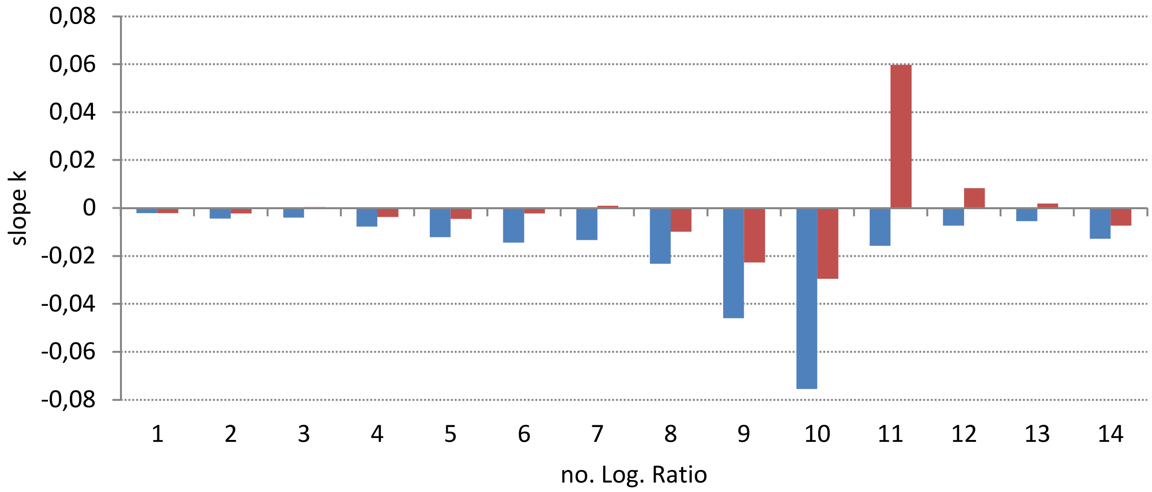

Fig 10.6, Distribution of slope values of the linear approximation of all 14 logarithmic ratios. Values represented by blue bars have been calculated on type A ratios, red bars belong to type B ratios

Following Eq. 10.1 – 10.4 the slopes k of the logarithmic ratios have to be negative. Increasing ratios with positive slopes results in a negative Q value, which is not feasible according to the theory of attenuation of seismic waves. Therefore the type B ratios in our example depicted in figure 10.6 turned out to be not reliable for Q value determination.

Q value

Once having a set of k's the quality factor Q can be calculated easily according to Eq. 10.4. The time difference $T\text{-}T_0$ is given by mean times of the corresponding stacked traces. The results of data analysis are presented and discussed in the next chapter.

10.3 RESULTS AND DISCUSSION OF THE SPECTRAL RATIO METHOD

The spectral ratio method has been applied to the VSP data set of the boreholes Strasshof T004 and Strasshof T006. Spectra of the seismic traces have been computed on different signal durations. A signal length of 70 ms at Strasshof T004 respectively 65 ms at Strasshof T006 covers one complete periodic cycle of the seismic wave. 150 ms signal duration encompasses the major part of energy recorded by the receiver and 950 ms is covering the entire signal of the trace.

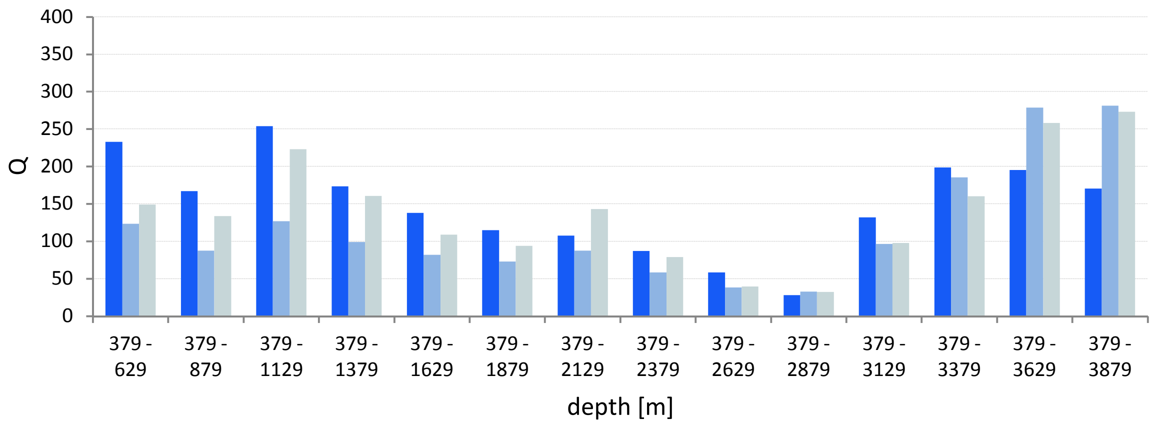

Fig. 10.7a. Q values type A of Strasshof T004, signal length is 70 ms (dark blue), 150 ms (light blue) and 950 ms (light grey)

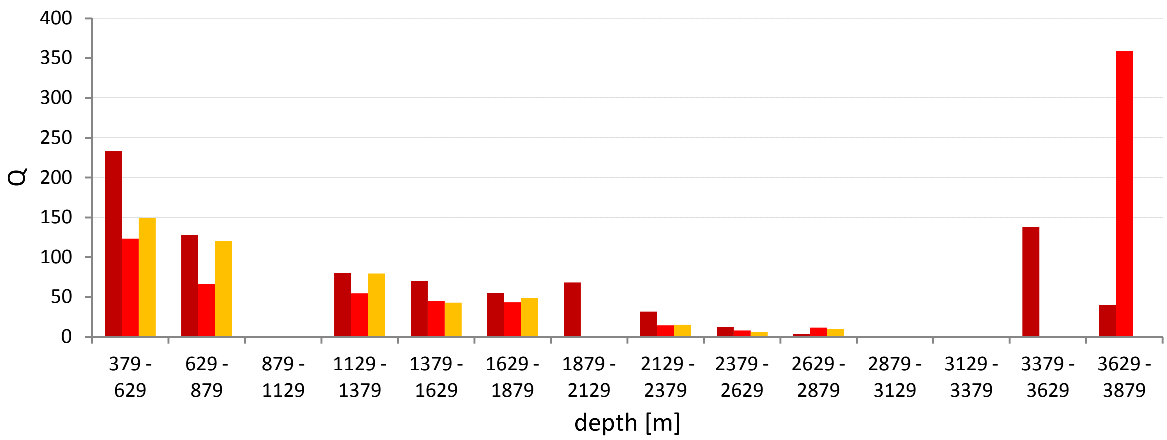

Fig 10.7b. Q values type B of Strasshof T004, signal length is 70 ms (dark red), 150 ms (light red) and 950 ms (orange). Missing data points result from negative Q values that have been deleted.

Fig. 10.7 illustrates the results of the data analysis of well Strasshof T004. Q values type A give an average attenuation related to the signal recorded at the shallowest level, whereas Q values type B can be considered to be the attenuation between two neighboring signals. Hence the distribution of type A values is expected to be smoother. Q values depicted in figure 10.7a are showing that the calculated quality factor varies with respect to the length of the signal used to compute the amplitude spectra. Varying the signal's length means changing the source signal, of course this leads to different results. Nevertheless the basic characteristic of value distribution does not change significantly. Q values obtained with signal duration of 70 ms, 150 ms and 950 ms correlate well with each other and can be found mainly within the expected Q value range between 50 and 400. Fig 10.7b gives the distribution of Q values type B. Some of the obtained quality factors are reaching values below zero. This means that longer wavelengths are affected stronger by attenuation than shorter wavelengths, which contradicts theoretical assumptions. Thus negative Q values have been interpreted as a consequence of measuring error.

In both diagrams a significant increase of Q values can be found in areas deeper than 3000 meters, these findings nicely correlates with the known boundary between Neogene and the Northern Calcareous Alps. The dolomite structures of the underneath Vienna Basin floor are supposed to have lower attenuation than the overlying sedimentary strata of the Neogene. In general, density as a consequence of compaction has a direct relationship to Q values, attenuation is assumed to be lower in highly compacted material because neighboring particles are interacting more directly (Lowrie 1997). Consequently one would expect Q values to increase with increasing depth, which is not evident in fig 10.7. Q values of 50 and below are much too low for depth of more than 2500 meters. OMNI 3D suggests quality factors values of 50 by default for surface rock. For highly compacted material in great depths value more than 100 are assumed. Hence the results of Q value analysis make further considerations necessary.

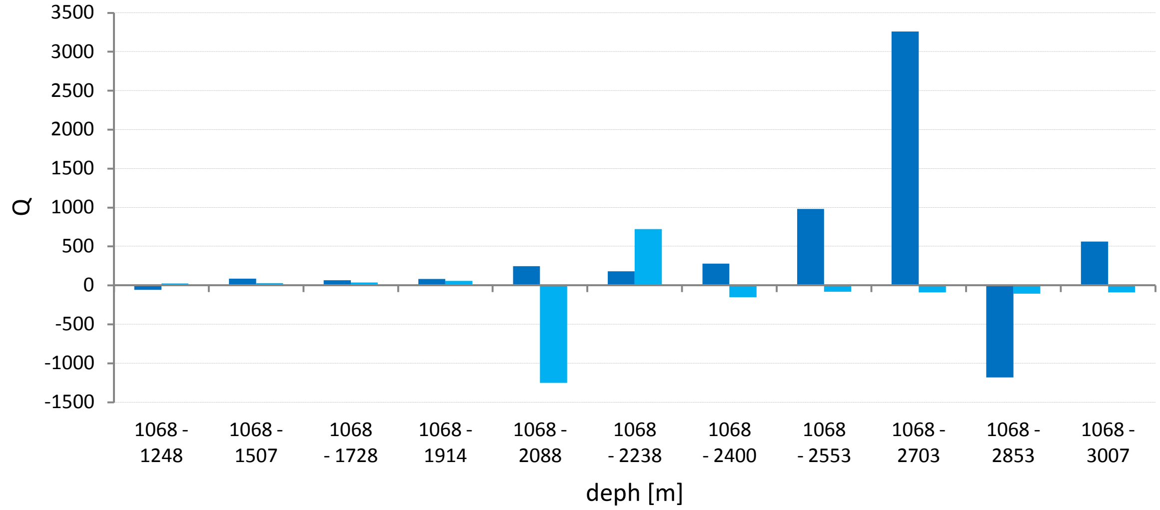

Fig. 10.8, Q values type A of Strasshof T006, signal length is 65 ms (dark blue) and 150 ms (light blue).

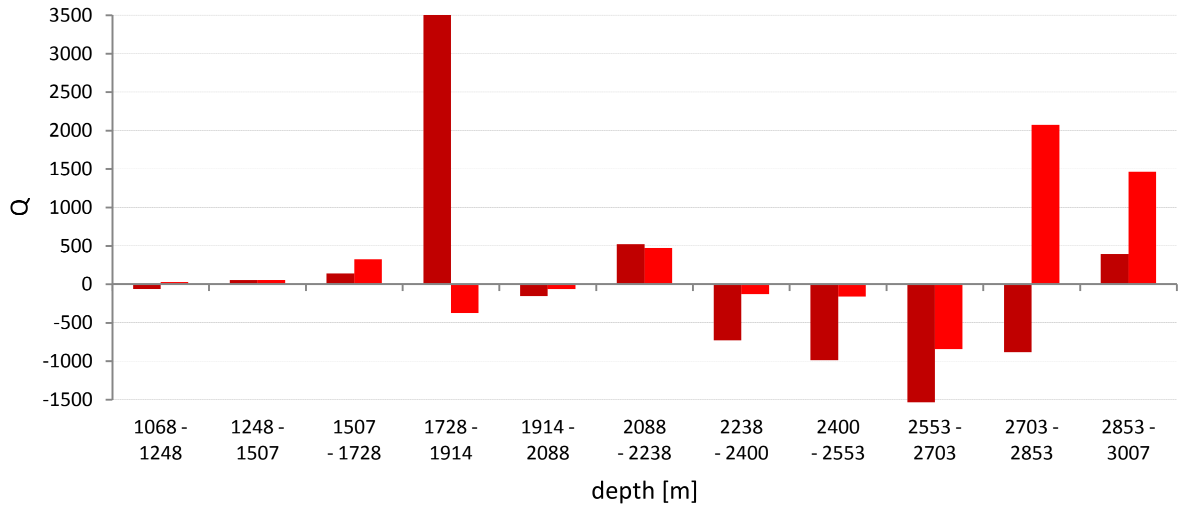

Fig. 10.8b, Q values type B of Strasshof T006, signal length is 65 ms (dark red), 150 ms (light red)

The Q values achieved from data analysis of well Strasshof T006 are depicted in fig 10.8 a-b. Spectra derived from traces with a signal duration of 950 ms turned out to be not analyzable because of poor data quality. Although the VSP data is available to a depth of 5400 meters, frequency ranges of linear decreasing ratios could not be found in corresponding depths below 3000 meters. But also evaluable traces recorded at shallower depth do not lead to stable results and can therefore not be used to quantify the absorption within the investigated area.

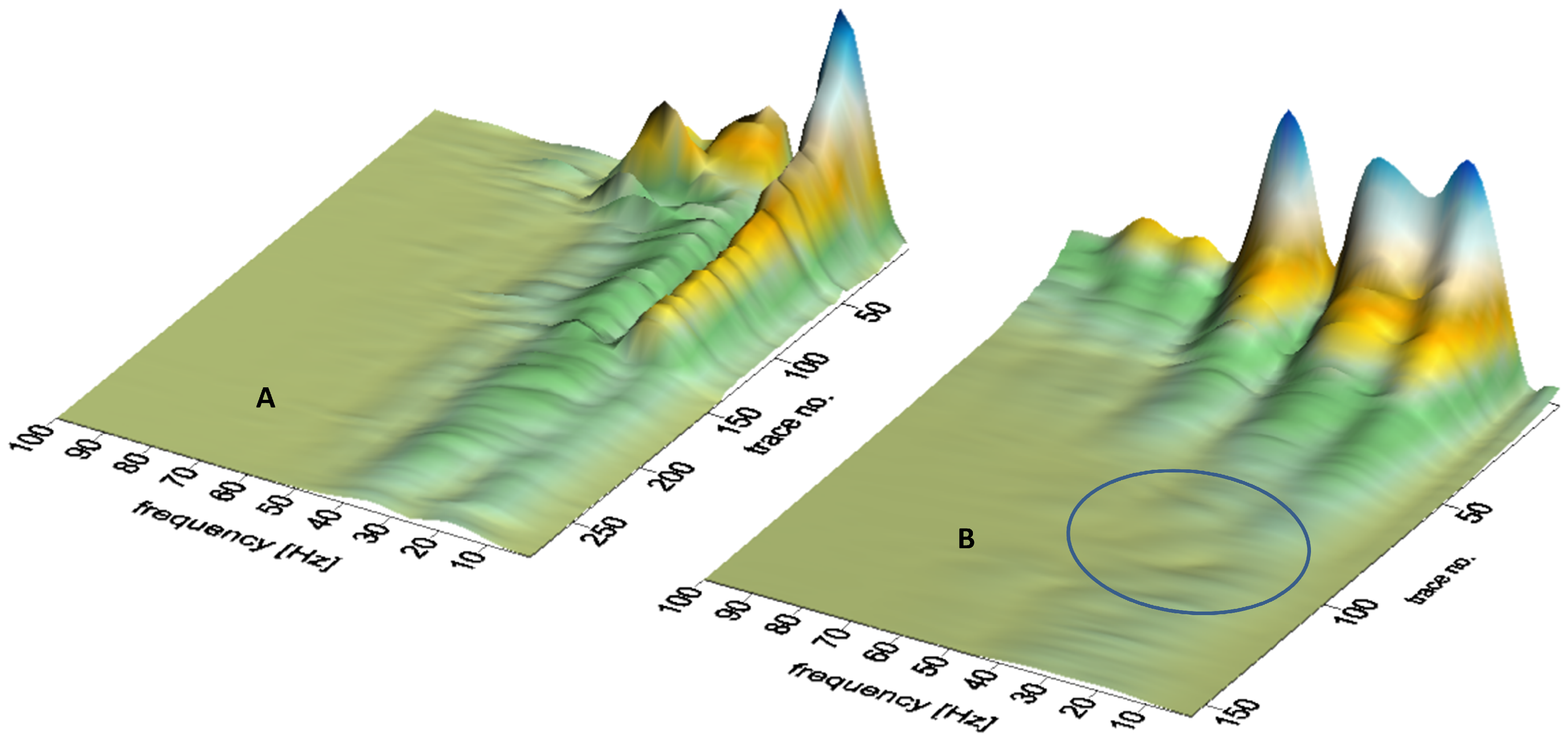

Fig. 10.9. 3d sketches of the amplitude spectra derived from VSP data of borehole Strasshof T006 (A) and Strasshof T004. Both data sets have been calculated from unstacked traces with a signal duration of 150 ms. The blue circle in B marks an area of vanishing amplitudes.

Amplitude spectra of both VSP data sets depicted in fig 10.9 could give an explanation for the poor and unstable results of Q value determination from Strasshof T006. Following De et al (1994) one of the demands on VSP data to be used for Q value determination is a constant source wave form between upper and lower levels. The amplitude spectra of Strasshof T006 (A) show prominent amplitudes in the frequency range between 10 Hz and 60 Hz at shallow levels. In deeper sections, beginning approximately trace 20 at a depth of 1315 meters, amplitudes within the frequency range from 30 Hz to 60 Hz are diminishing rapidly. In contrary, lower frequencies are showing the expected smooth amplitude decrease. At a depth of approximately 3500 meters, which corresponds to trace 140, the amplitude of the prominent 15 Hz ridge decreases rapidly. Thus, the assumption of constant source wave form for every trace is not valid anymore. The VSP data set of well Strasshof T006 does not meet the strict requirements on data quality and is therefore not evaluable regarding Q value determination. The amplitude spectra of Strasshof T004 (fig 10.9 B) shows the continuously decreasing amplitudes within the whole frequency range. The blue circle marks an area where amplitudes seem to diminish within a certain depth range.

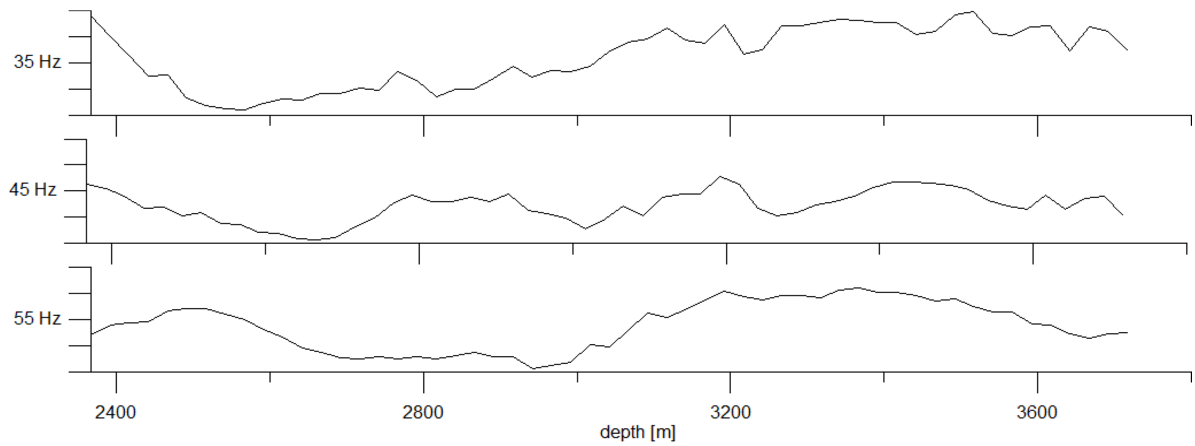

Fig 10.10, Amplitudes of selected frequencies between within 2400 meters and 3600 meters depth. The range of low amplitudes between 2500 meters and 3000 meters corresponds nicely with the area marked with the blue circle in fig 10.9.

Amplitudes depicted in fig 10.10 are showing the sudden decay of amplitudes at approximately between 2400 meter and 2600 meters depth. In depths between 2800 meters and 3000 meters the amplitudes increase again to a similar level. Calculating the logarithmic ratio type B for this depth would give positive slope values. The depths of positive slope values shown in fig 10.6 are correlating well with the depths of irregularly changing amplitudes.

$$A_Z = A_0 \times \frac{Z_0}{Z}$$

Assuming a constant waveform over the entire depth range, the amplitudes are supposed to decrease continuously with depth. The occurrence of diminishing and rising amplitudes can be explained with variations of the coupling between receivers and the adjacent rock. A reason for this could be a change of lithology or texture of rock material. A constant geophone coupling is one of the demands on data quality defined in chapter 10.1. Obviously the VSP data set of well Strasshof Tief 004 does not fully meet these requirements. A Q value analysis using the spectral ratio method is therefore not feasible.

10.4 SPECTRAL MODELLING

Although the VSP data coming from well Strasshof T004 does not fulfill the demands on data quality due to uncertainties in geophone coupling, it still shows the expected characteristics and seems to meet the rest of the requirements as defined in chapter 10.1. This gives rise to the spectral modelling method, which is based on the idea to compute a set of artificially attenuated amplitude spectra from actually measured spectra. Subsequent comparison with real spectra and adaption of attenuation by varying the Q values leads to the best fitting result.

Spectral modelling follows two main steps:

1. Computing artificial spectra and correction of geometrical spreading
2. Applying frequency dependent attenuation

<u>Computing artificial spectra and applying geometrical effects</u>

Spherical divergence is assumed to be independent on frequency and follows an inverse relationship between amplitude and the distance from the point of origin. The amplitude spectrum A_Z at depth Z can be calculated from a reference spectrum A_0 at a reference level Z_0.

$$A_Z = A_0 \times \frac{Z_0}{Z} \qquad \text{(Eq. 10.5)}$$

The reference amplitude spectrum has been calculated from the shallowest trace of the VSP data set of borehole Strasshof T004 and corresponds to a depth of 266 meters.

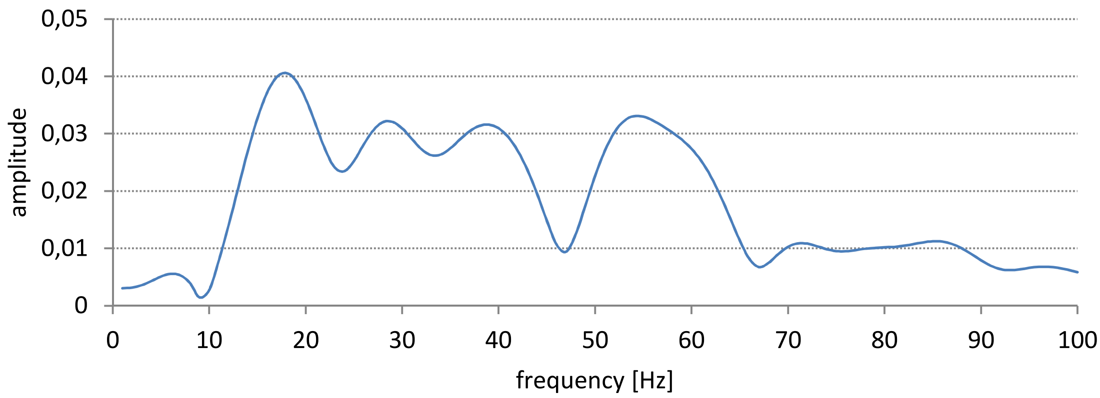

Fig 10.11, Reference amplitude spectrum, signal length is 150 milliseconds

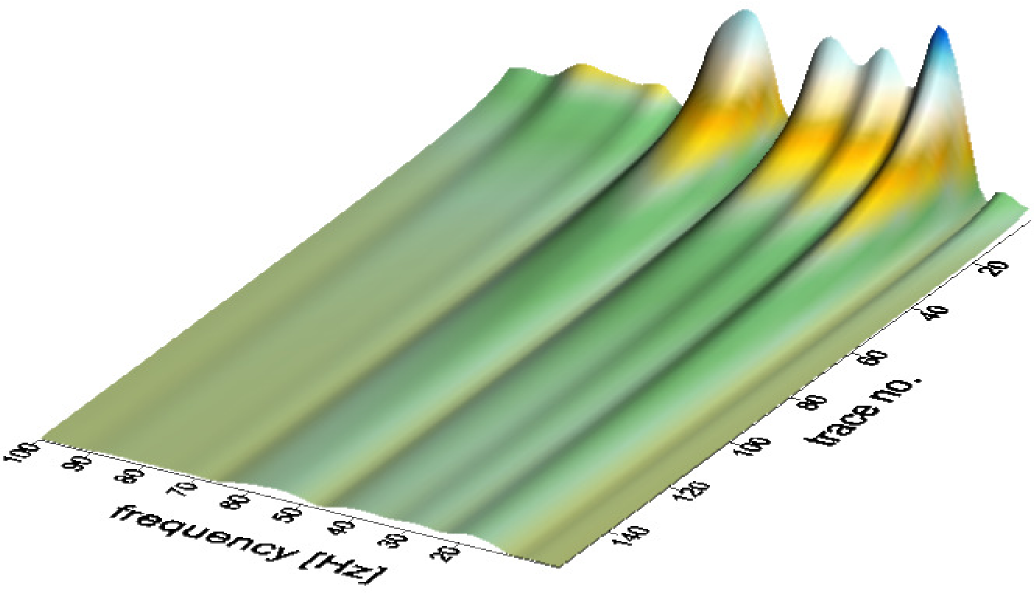

Fig 10.12, Geometrical spreading effect applied to artificial set of amplitude spectra.

Applying frequency dependent attenuation

The final attenuation model will be defined along three sections of different Q values. The boundaries between these sections are defined by the surfaces of the structural model. The uppermost one is ranging from the subsurface down to the bottom surface of the *Sandschaller zone* at a depth of approximately *1400 meters*. The section underneath reaches from the Sandschaller zone to *Neogene basin floor* at a depth *of 2800 meters*. The third and undermost section is given by the *Northern Calcareous Alps*. Eq. 10.2 establishes the basis for the spectra modeling method and leads to:

$$A(Z, f) = A(Z_0, f).\exp\frac{-\pi f(T - T_0)}{Q} \qquad \text{(Eq. 10.6)}$$

A set of three Q values assigned to the corresponding depths is applied to the artificial amplitude spectra. Subsequent comparison with the real data set leads to an iterative adaption of the Q values.

Fig 10.13 shows the amplitudes along the 40 Hz line. The blue dotted graph represents amplitudes only damped with geometrical effect, which clearly illustrates that the major part of signal decrease is caused by spherical divergence. Applying synthetical attenuation according to the Q start model gives the red line, where amplitudes still have too high values. The start model is based on Q values for compacted sedimentary rock suggested by Schön (1996). Iteratively performed Q value adaption and comparison lead to the final model (green), which gives a nicely fitting result over the whole frequency range (fig 10.14).

The logarithmic depiction in fig 10.13b shows clearly the sudden decay of amplitude at a depth of approximately 2400 meters. This is also evident in fig. 10.9 and fig 10.10 and is identified as a probable consequence of poor coupling between geophone and the adjacent rock. The fact that the final attenuation model (green) represents the general trend of amplitude decay of real data sufficiently well gives support to the assumption that energy loss caused by reflection is negligible. Therefore the decision not to consider the amplitude loss at reflecting interfaces for Q value analysis seems to be arguable.

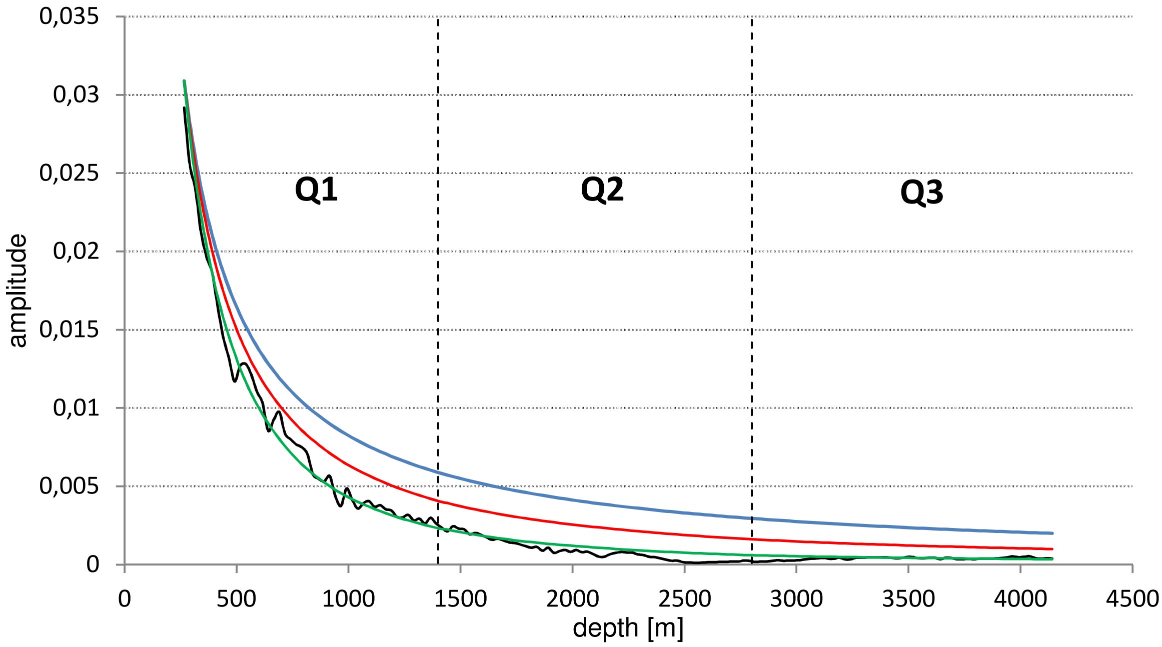

Fig 10.13a, Amplitude decay of 40 Hz frequency of well Strasshof T004.(linear scale)

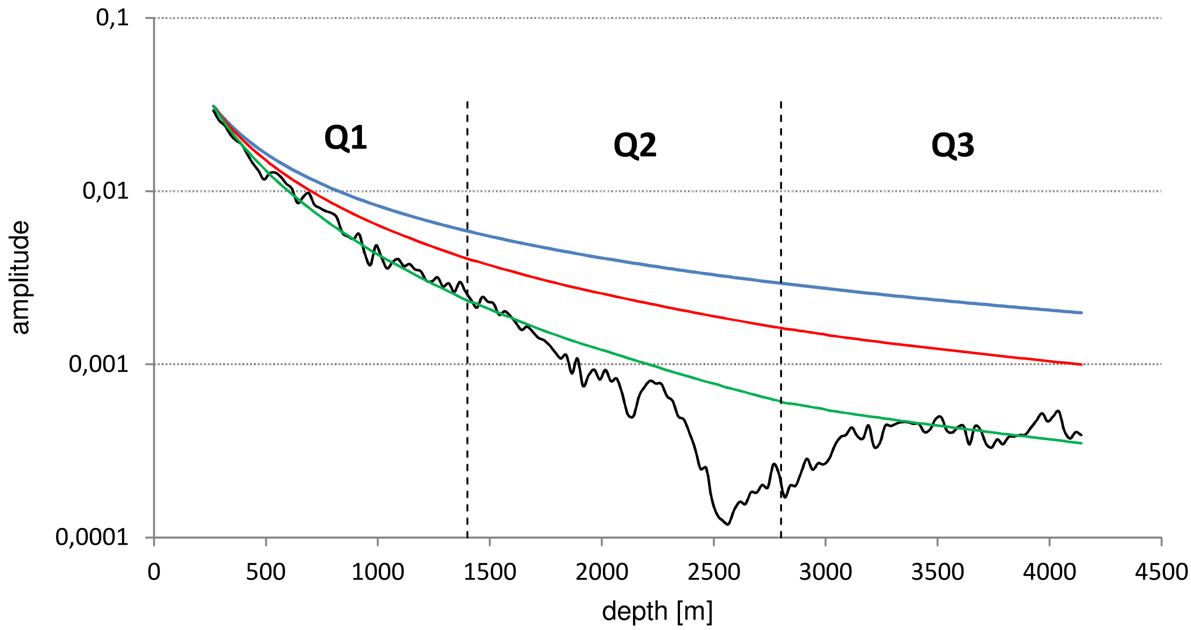

Fig 10.13b, Amplitude decay of 40 Hz frequency of well Strasshof T004.(logarithmic Y-scale)

Fig 10.13a-b, Amplitude decay of 40 Hz frequency. The black scattered line represents actually measured data. The effect of spherical divergence only is illustrated by the blue line. The green and red lines give the result of artificially applied attenuation with two different Q models given in table 10.2. The dotted vertical lines are separating the 3 areas of different Q values

	depth	trace	Q start model (red)	Q final model (green)
Q1	266 - 1391	1 - 47	150	60
Q2	1416 - 2791	48 - 103	200	70
Q3	2816 - 4141	103 - 156	300	180

Tab 10.2, Q model parameter synthetically applied attenuation. The Q values of the final model are the result of iterative improvement and define the attenuation within the investigated area.

Compared to results of the spectral ratio method the Q values achieved from spectral modeling are more reliable and in accord to values suggested in literature (Schön 1996). It is notable that a wide range of values leads to sufficiently good correlation between computed and real data especially in deeper sections. E.g. changing the Q value for the Northern Calcareous Alps from 180 to 400 leads not to a difference in results that can be proven reliably by comparison between the two data sets.

The obtained set of attenuation parameter has been implemented into the velocity model according to the data format requirements of OMNI 3D defined in chapter 9.3. Hence information on the attenuation and the velocity distribution is linked together in one final model.

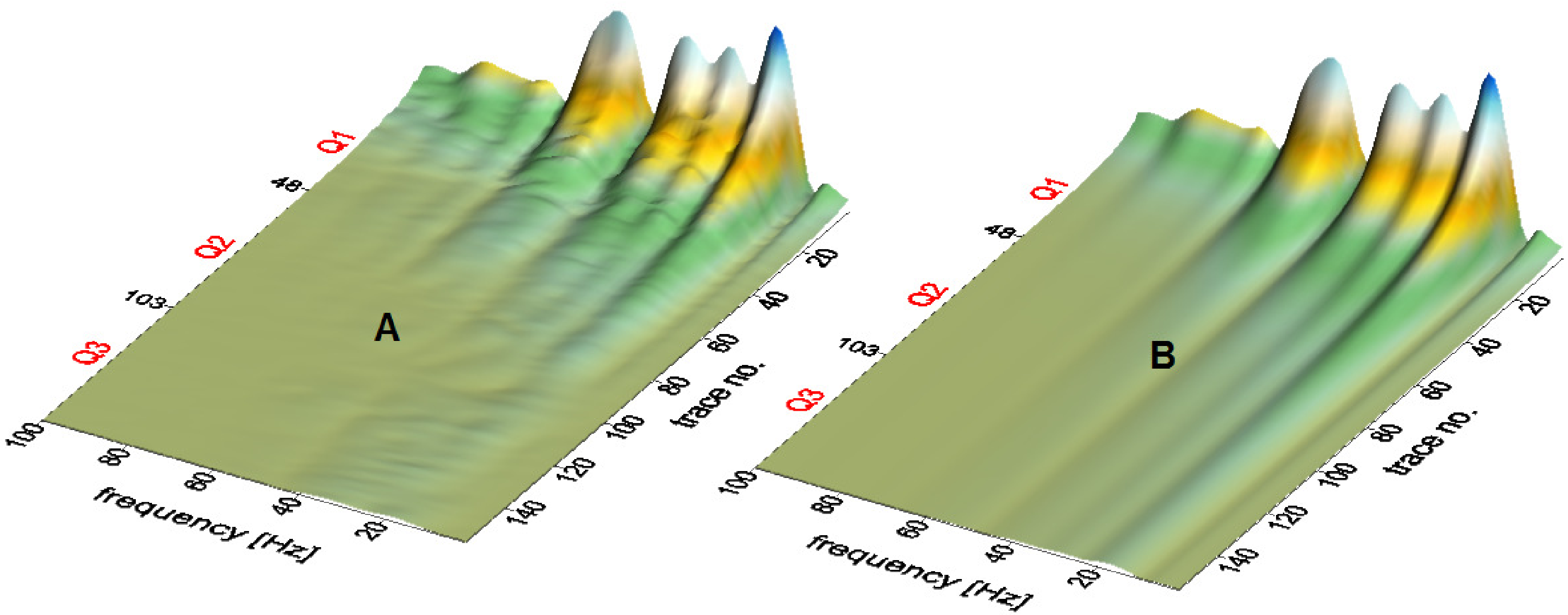

Fig. 10.14, 3D sketches of the amplitude spectra of well Strasshof T004, comparison between real data (A) and calculated data using spectral modeling (B). Iterative improvement and adaption of the Q values leads to an artificial set of amplitude spectra that nicely correlate with the amplitude spectra of actually measured data. Q1, Q2 and Q 3 are marking the three areas of different attenuation

11 CONCLUSIONS

The two main blocks of the final model, representing the Neogene and the underlying Northern Calcareous Alps, are designed following two different approaches. Due to the availability of a qualified data base of the Neogene Basin fill the upper part of the model encompasses already known and proven information. Due to the lack of accurate information on the deep Vienna Basin the construction of the lower part of the model is based on a preliminary understanding of the deep buried formations, the implementation of partly given horizons and the analysis of well data coming from selected boreholes.

The 3D PSDM velocity field shows good correlation between velocity discontinuities and checkshot velocities. Thus, the three-dimensional velocity distribution of the upper part model is established by a given velocity cube. The structural model of the Neogene is defined by five surfaces that are covering the entire area of interest and are proven by high number of boreholes, which give the exact location of tops and bottoms of the corresponding formations.

The boundary between the upper and the lower part of the model is established by basin floor of the Neogene. For the internal structure of the Northern Calcareous Alps only three surfaces derived from seismic data are given, which are covering the horizontal plan just partly. Covering the whole area of interest is one of the demands for surfaces to be used for setting up velocity model. In order to fulfill this requirement the surfaces have been extended in line with the general understanding of the deep Vienna Basin. To define the complete buildup of the internal structure individual surfaces like the base of the *Frankenfelser-Lunzer nappe* or the base of the *Giesshübler monocline* have to be generated without any relation to clear seismic reflections or support of well data. The interpretation of these horizons on seismic sections is just a rough estimation and would not have been possible without the aid of OMV expert knowledge.

In order to define the velocity distribution sonic log data and checkshot data have been utilized. The challenge was to combine these two sets of velocity data that originate from different methods, depths and lithologies. A special focus was set on the velocity increase as a consequence of compacted rock in greater depth.

To determine the velocity gradient within a certain formation, data points all over the vertical extension of the corresponding geological unit would be desirable. Unfortunately none of the available wells meets this demand, e.g. borehole Strasshof T002 provides approximately 60 vertical meters of sonic log data of the Frankenfelser-Lunzer nappe. Comparing this to the total thickness of more than 2000 meters, the difficulties in estimating the vertical velocity distribution for the entire formation becomes obvious.

Setting up an interval velocity model with PETREL 2009 only allows assigning constant velocity values or linear increasing values within a defined area. The velocity gradient in great depths as a consequence of compaction will of course not be constant, even more in the presence of heterogeneous lithologies, but one has to deal with the limitations of the used software. Calculating a linear regression of the measured velocity values leads to a first grade polynomial that represents the velocity increase sufficiently within the considered vertical range. As compaction cannot occur infinitely, the linear velocity increase is stopped in a depth of approximately 6200 meters and turns into a constant value. Once more the definition of this depth is based on the estimations of OMV experts.

The third parameter of the model is the seismic quality factor Q, which was determined by analyzing the VSP data of two selected boreholes. The initially chosen approach was the spectral ratio method, which led to unstable and therefore not reliable Q values. Data analysis and three-dimensional visualization give a possible explanation for the poor results. According to De et al (1994) one of the demands on data quality when applying the spectral ration method is that the source wave form has to be constant within the investigated area. The results clearly illustrates that the assumption of a constant wave form is not valid for the used VSP data. The reason for this could be that the initial intention of the VSP surveys was not to acquire data for Q value analysis, therefore the focus during the acquisition was not to ensure a constant wave form but to enhance the signal to noise ratio. Varying numbers of shots have been stacked to one single trace which makes the constant source assumption obsolete. Applying the spectral modeling method led to stable results that are in accord with Q values suggest in literature (Schoen 1996).

To conclude shortly on Q value determination: VSP data to be used for attenuation analysis has to follow strict requirements on data quality, the VSP data acquisition survey has to be especially designed for Q value analysis to be performed later on.

If the spectral ratio method is not appropriate the spectral modeling method can give an alternative under the limitation that the variation of the source wave form is small to moderate.

Comprehensive velocity models that contain attenuation and structural information as well may play a key role for the configuration of a target oriented seismic acquisition survey. The quality of the model depends largely on the amount and on the quality of data on which it is based on.

11 ACKNOWLEDGEMENTS

I want to thank OMV Exploration & Production and in particular Dr. Roman Spitzer and Dr. Christian Stotter for providing me with this topic and support me during the practical work.
Overall thanks go to my family for supporting and encouraging me during my studies and especially to Michaela Glanz for motivating me in times of hard work and guiding me through linguistic challenges. And of course I am very grateful to Prof. Dr. Ewald Brückl, under whose supervision this thesis was conducted.

.

13 REFERENCES

Aki, K., Richards P.G. (2002), Quantitative seismology, 2nd edition, University science books, Sausalito, CA

Brix, F., Schultz, O. (1993), Erdöl und Erdgas in Österreich, 2te Auflage

De, G.S., Winterstein, D.F., Meadows, M.A. (1994), Comparison of P-and S-wave velocities and Q´s from VSP and sonic log data, Geophysics, Vol.59, 1512-1529

Faust, L.Y., (1953), A velocity function including lithologic variation: Geophysics Vol 18, 271–288, cited in Sherriff, R. (2002), Encyclopedic Dictionary of Applied Geophysics, 4th Edition, Geophysical references No. 13 SEG

Fuchsluger, M., Pfeiler, S., Stotter, C., Chwatal, W., Brückl, E., (2011), 3D model based seismic acquisition design for imaging the deep Vienna Basin (Poster). 73rd EAGE Conference and Exhibition incorporating SPE EUROPEC 2011 Vienna, Austria.

Gladwin, M.T., Stacey, F.D. (1974), Anelastic degradiation of acoustic pulses in rock, Physics of the Earth and Planetary Interiors 8, 332-336, cited in Tonn, R. (1991), The determination of the seismic quality factor Q from VSP data: a comparison of different computational methods, Geophysical Prospecting 39, 1-27

Hamilton, W., Wagner, L., Wessely, G. (1999), Oil and Gas in Austria, Mitteilungen der Österreichischen geologischen Gesellschaft, 92, 235-262

Jaeger, R., Mann, J., Hoecht, G., Hrubal, P. (2001), Common-reflection-stack: Image and attributes, Geophysics Vol. 66, 97-109

Kreutzer, N. (1993), Das Neogen des Wiener Beckens, in: Brix, F., Schultz, O. (Hg.), Erdöl und Erdgas in Österreich, 2te Auflage, S 232-248.

Lowrie, W. (1997), Fundamentals of Geophysics, 2nd Edition, Cambridge University Press

Milsom, J. (2003), Field Geophysics, 3rd Edition, Wiley, 197-206

Piller, W.E., (1999), The Neogene of the Vienna Basin, FOREGS '99

Rögl, F. (1999), Mediterrean and Paratethys. Facts an Hypotheses of an oligocene to miocene paleogeography (Short overview), Geologica carpthica, 50, 4, Bratislava, Aug. 1999, 339-349

Royden, L.H. (1985), The Vienna Basin: A thin-skinned pull-apart basin. In: Biddle, K.T. and Christieblik, N.: Strike slip deformation, basin formation and sedimentation. Society of Economic Paleontologists and Mineralogists, Special Publication 37, 319-338

Royden, L.H., Horvath, F. (1988), The Pannonian System - A study in basin evolution. Amer. Assoc. Petrol. Geol. Mem. 45, Tulsa - Oklahoma.

Schlumberger Ltd. (2012), www.glossary.oilfield.slb.com/Display.cfm?Term=check-shot%20survey, (May 2012)

Schön, J.H. (1996), Physical properties of rocks: Fundamentals and principles of petrophysics, Elsevier

Sherriff, R. (2002), Encyclopedic Dictionary of Applied Geophysics, 4th Edition, Geophysical references No. 13 SEG

Stainsby S.D., Worthington M.H. (1985), Q estimation from vertical seismic profile data and anomalous variations in the central North Sea, Geophysics, Vol. 50, 615-626

Telford, W.M., Geldart L.P., Sheriff R.E. (1990), Applied Geophysics, 2nd Edition, Cambridge University Press

Tonn, R. (1991), The determination of the seismic quality factor Q from VSP data: a comparison of different computational methods, Geophysical Prospecting 39, 1-27

Wessely, G. (1988), Structure and Development of the Vienna Basin in Austria, in: Royden, L.H. and Horvath, F.: The Pannonian System - A study in basin evolution. Amer. Assoc. Petrol. Geol. Mem. 45, Tulsa - Oklahoma.

Wessely, G. (1993), Der Untergrund des Wiener Beckens, in: Brix, F., Schultz, O. (Hg.), Erdöl und Erdgas in Österreich, 2te Auflage, S 249-280.

Wessely, G. (2006), Geologie der österreichischen Bundesländer – Niederösterreich, Geologische Bundesanstalt Wien

Yilmaz, Ö. (2001), Seismic Data Analysis, Processing, Inversion and Interpretation of Seismic Data, Volume 1 + 2, SEG

STEFAN PFEILER

stefanpfeiler@gmx.net

Personal Data

Date of birth:	03. May 1976
Place of birth:	Feldbach / Steiermark
Nationality:	Austria
Martial status:	unmarried

Education

2004.– 2012:	Master's degree in Geophysics at the University of Vienna
1999 – 2003:	Institution for higher education for electrical engineering, graduating with Matura (A –levels, graduation diploma) at BULME Graz
1992 – 1996:	Apprenticeship as electromechanic at AVL List Graz
1990 – 1992:	Institution for higher education for electrical engineering Weiz
1982 – 1990:	Elementary and secondary school in Feldbach

Military service

1996 – 1997:	Military service at Montecucolli casern in Güssing

Work experience

Since 2010: Employment at the Geological Survey of Austria
Application of geoelectrical methods in landslide and permafrost monitoring
2007 – 2010: Service contract at Geological Survey of Austria
Implementation of geoelectrical and borehole measurements
1996 – 2004: Employment AVL List GmbH
Electrical engineer for service and maintenance

1992-1996 Apprenticeship in electro mechanics, AVL List GmbH

Language skills

German (native)
English (good)

Computer literacy

MS Windows and Office, C, C++, MatLab, Octave, ArcGis